



1        **Marine organic matter in the remote environment of the Cape Verde**  
2        **Islands – An introduction and overview to the MarParCloud campaign**

3

4        Manuela van Pinxteren<sup>1\*</sup>, Kanneh Wadinga Fomba<sup>1</sup>, Nadja Triesch<sup>1</sup>, Christian Stolle<sup>2,3</sup>,  
5        Oliver Wurl<sup>3</sup>, Enno Bahlmann<sup>2,4</sup>, Xianda Gong<sup>1</sup>, Jens Voigtländer<sup>1</sup>, Heike Wex<sup>1</sup>, Tiera-  
6        Brandy Robinson<sup>3</sup>, Stefan Barthel<sup>1</sup>, Sebastian Zeppenfeld<sup>1</sup>, Erik H. Hoffmann<sup>1</sup>, Marie  
7        Roveretto<sup>5</sup>, Chunlin Li<sup>5</sup>, Benoit Grosseclin<sup>6</sup>, Veronique Daële<sup>6</sup>, Fabian Senf<sup>1</sup>, Dominik van  
8        Pinxteren<sup>1</sup>, Malena Manzi<sup>7</sup>, Nicolás Zabalegui<sup>7</sup>, Sanja Frka<sup>8</sup>, Blaženka Gašparović<sup>8</sup>, Ryan  
9        Pereira<sup>9</sup>, Tao Li<sup>10</sup>, Liang Wen<sup>10</sup>, Jiarong Li<sup>11</sup>, Chao Zhu<sup>11</sup>, Hui Chen<sup>11</sup>, Jianmin Chen<sup>11</sup>, Björn  
10       Fiedler<sup>12</sup>, Wolf von Tümpling<sup>13</sup>, Katie A. Read<sup>14</sup>, Shalini Punjabi<sup>14,15</sup>, Alastair C. Lewis<sup>14,15</sup>,  
11       James R. Hopkins<sup>14</sup>, Lucy J. Carpenter<sup>15</sup>, Ilka Peeken<sup>16</sup>, Tim Rixen<sup>4</sup>, Detlef Schulz-Bull<sup>2</sup>,  
12       María Eugenia Monge<sup>7</sup>, Abdelwahid Mellouki<sup>6,10</sup>, Christian George<sup>5</sup>, Frank Stratmann<sup>1</sup>,  
13       Hartmut Herrmann<sup>1,10\*</sup>

14

15       \*corresponding authors: Manuela van Pinxteren (manuela@tropos.de) and Hartmut Herrmann  
16       ([herrmann@tropos.de](mailto:herrmann@tropos.de))

17

18

19       <sup>1</sup> Leibniz-Institute for Tropospheric Research (TROPOS), 04318 Leipzig, Germany

20       <sup>2</sup> Leibniz-Institute for Baltic Sea Research Warnemuende, 18119 Rostock, Germany

21       <sup>3</sup> Institute for Chemistry and Biology of the Marine Environment, Carl-von-Ossietzky  
22       University Oldenburg, 26382 Wilhelmshaven, Germany

23       <sup>4</sup> Leibniz Centre for Tropical Marine Research (ZMT), 28359 Bremen, Germany

24       <sup>5</sup> Institut de Recherches sur la Catalyse et l'Environnement de Lyon, Lyon, France.

25       <sup>6</sup> Institut de Combustion, Aérothermique, Réactivité et Environnement, Centre National de la  
26       Recherche Scientifique, Orléans, France.

27       <sup>7</sup> Centro de Investigaciones en Bionanociencias (CIBION), Consejo Nacional de Investigaciones  
28       Científicas y Técnicas (CONICET), C1425FQD, Ciudad de Buenos Aires, Argentina

29       <sup>8</sup> Division for Marine and Environmental Research, Ruđer Bošković Institute, 10000 Zagreb, Croatia

30       <sup>9</sup> Lyell Centre, Heriot-Watt University, EH14 4AP, Edinburgh, United Kingdom

31       <sup>10</sup> School of Environmental Science and Engineering, Shandong University, Qingdao 266237, China

32       <sup>11</sup> Shanghai Key Laboratory of Atmospheric Particle Pollution and Prevention, Institute of

33       Atmospheric Sciences, Fudan University, Shanghai, 200433, China

34       <sup>12</sup> GEOMAR Helmholtz Centre for Ocean Research, Kiel, Germany

35       <sup>13</sup> Helmholtz Centre for Environmental Research - UFZ, 39114, Magdeburg, Germany

36       <sup>14</sup> National Centre for Atmospheric Science (NCAS), University of York, Heslington, York, YO10  
37       5DD

38       <sup>15</sup> Wolfson Atmospheric Chemistry Laboratories, Department of Chemistry, University of York,  
39       Heslington, York, YO10 5DD

40       <sup>16</sup> Alfred-Wegener-Institute Helmholtz Centre for Polar and Marine Research, Bremerhaven, Germany

41

42

43

44

45

46



47 Abstract

48

49 The project MarParCloud (Marine biological production, organic aerosol Particles and marine  
50 Clouds: a process chain) aims at improving our understanding of the genesis, modification and  
51 impact of marine organic matter (OM), from its biological production, via its export to marine  
52 aerosol particles and, finally, towards its ability to act as ice nucleating particles (INP) and  
53 cloud condensation nuclei (CCN). A field campaign at the Cape Verde Atmospheric  
54 Observatory (CVAO) in the tropics in September/October 2017 formed the core of this project  
55 that was jointly performed with the project MARSU (MARine atmospheric Science  
56 Un unravelled). A suite of chemical, physical, biological and meteorological techniques was  
57 applied and comprehensive measurements of bulk water, the sea surface microlayer (SML),  
58 cloud water and ambient aerosol particles collected at a ground-based and a mountain station  
59 took place.

60 Key variables comprised the chemical characterization of the atmospherically relevant OM  
61 components in the ocean and the atmosphere as well as measurements of INP and CCN.  
62 Moreover, bacterial cell counts, mercury species and trace gases were analysed. To interpret  
63 the results, the measurements were accompanied by various auxiliary parameters such as air  
64 mass back trajectory analysis, vertical atmospheric profile analysis, cloud observations and  
65 pigment measurements in seawater. Additional modelling studies supported the experimental  
66 analysis.

67 During the campaign, the CVAO exhibited marine air masses with low and partly moderate  
68 dust influences. The marine boundary layer was well mixed as indicated by an almost uniform  
69 particle number size distribution within the boundary layer. Lipid biomarkers were present in  
70 the aerosol particles in typical concentrations of marine background conditions. Accumulation  
71 and coarse mode particles served as CCN and were efficiently transferred to the cloud water.  
72 The ascent of ocean-derived compounds, such as sea salt and sugar-like compounds, to the  
73 cloud level as derived from chemical analysis and atmospheric transfer modelling results denote  
74 an influence of marine emissions on cloud formation. However, INP measurements indicated  
75 also a significant contribution of other non-marine sources to the local INP concentration or  
76 strong enrichment processes during upward transport. In addition, the number of CCN at the  
77 supersaturation of 0.30% was about 2.5 times higher during dust periods compared to marine  
78 periods. Lipids, sugar-like compounds, UV absorbing humic-like substances and low molecular  
79 weight neutral components were important organic compounds in the seawater and highly  
80 surface-active lipids were enriched within the SML. The selective enrichment of specific  
81 organic compounds in the SML needs to be studied in further detail and implemented in an OM  
82 source function for emission modelling to better understand transfer patterns, mechanisms of  
83 marine OM transformation in the atmosphere and the role of additional sources.

84 In summary, when looking at particulate mass, we do see oceanic compounds transferred to the  
85 atmospheric aerosol and to the cloud level, while from a perspective of particle number  
86 concentrations, marine contributions to both CCN and INP are rather limited.

87

88



89 **Keywords**

90 MarParCloud, MARSU, organic matter, seawater, sea surface microlayer, aerosol particles,  
91 cloud water, Cape Verde Atmospheric Observatory (CVAO)

92 **1 Introduction and Motivation**

93 The ocean covers around 71% of the earth's surface and acts as a source and sink for  
94 atmospheric gases and particles. However, the complex interactions between the marine  
95 boundary layer (MBL) and the ocean surface are still largely unexplored (Cochran, et al. 2017;  
96 de Leeuw, et al. 2011; Gantt and Meskhidze 2013; Law, et al. 2013). In particular, the role of  
97 marine organic matter (OM) with its sources and contribution to marine aerosol particles, is still  
98 poorly understood, where this particle fraction might lead to a variety of effects such as  
99 changing health effects, changing radiative properties, changing effects of marine particles  
100 deposited to the ecosystems (e.g. Abbatt, et al. 2019; Brooks and Thornton 2018; Burrows, et  
101 al. 2013; Gantt and Meskhidze 2013; Pagnone, et al. 2019). Furthermore, knowledge on the  
102 properties of marine organic aerosol particles and their ability to act as cloud condensation  
103 nuclei (CCN) or ice nucleating particle (INP) is still elusive. Ocean-derived INPs were  
104 suggested to play a dominating role in determining INP concentrations in near-surface-air over  
105 the remote areas such as the Southern Ocean, however their source strength in other oceanic  
106 regions is still largely unknown (Burrows, et al. 2013; McCluskey, et al. 2018a; McCluskey, et  
107 al. 2018b).

108 During recent years, it was clearly demonstrated that marine aerosol particles contain a  
109 significant organic mass fraction derived from primary and secondary processes (Middlebrook,  
110 et al. 1998; Prather, et al. 2013; Putaud, et al. 2000; van Pinxteren, et al. 2017; van Pinxteren,  
111 et al. 2015). Although it is known that the main OM groups show similarities to the oceanic  
112 composition and comprise carbohydrates, proteins, lipids as well as humic-like and refractory  
113 organic matter, a large fraction of OM in the marine environment is still unknown on a  
114 molecular level (e.g. Gantt and Meskhidze 2013).

115 The formation of ocean-derived aerosol particles and their precursors is influenced by the  
116 uppermost layer of the ocean, the sea surface microlayer (SML) formed due to different  
117 physicochemical properties of air and water (Engel, et al. 2017; Wurl, et al. 2017). Recent  
118 investigations suggest that the SML is stable up to wind speeds of  $> 10 \text{ m s}^{-1}$  and is therefore  
119 existent at the global average wind speed of  $6.6 \text{ m s}^{-1}$  and a fixed component influencing the  
120 ocean atmosphere interaction on global scales (Wurl, et al. 2011). The SML is involved in the  
121 generation of sea-spray (or primary) particles including their organic fraction by either transfer  
122 of OM to rising bubbles before they burst out or through a more direct transfer of OM from the  
123 ocean compartments to the marine particles. A mechanistic and predictable understanding of  
124 these complex and interacting processes is still lacking (e.g. Engel, et al. 2017). Moreover,  
125 surface films influence air-sea gas exchange and may undergo (photo)chemical reactions  
126 leading to a production of unsaturated and functionalized volatile organic compounds (VOCs)  
127 acting as precursors for the formation of secondary organic aerosol (SOA) particles  
128 (Brueggemann, et al. 2018; Ciuraru, et al. 2015). Thus, dynamics of OM and especially surface-  
129 active compounds present at the air-water interface may have global impacts on the air-sea



130 exchange processes necessary to understand oceanic feedbacks on the atmosphere (e.g. Pereira,  
131 et al. 2018).

132 Within the SML, OM is a mixture of different compounds such as polysaccharides, amino acids,  
133 proteins, lipids and it occurs as particulate and chromophoric dissolved organic matter (CDOM)  
134 (e.g. Gašparović, et al. 1998a; Gašparović, et al. 2007; Stolle, et al. 2019). In addition, the  
135 complex microbial community is assumed to exert a strong control on the concentration and  
136 the composition of OM (Cunliffe, et al. 2013). In calm conditions, bacteria accumulate in the  
137 SML (Rahlff, et al. 2017) and are an integral part of the biofilm-like habitat forming at the air-  
138 sea interface (Stolle, et al. 2010; Wurl, et al. 2016).

139 A variety of specific organic compounds such as surface-active substances (SAS), volatile  
140 organic compounds (VOC), and acidic polysaccharides aggregating to transparent exopolymer  
141 particles (TEP), strongly influence the physico-chemical properties of OM in the SML. SAS  
142 (or surfactants) are highly enriched in the SML relative to bulk water and contribute to the  
143 formation of surface films (Frka, et al. 2009; Frka, et al. 2012; Wurl, et al. 2009). SAS are  
144 excreted by phytoplankton, during zooplankton grazing and bacterial activities (e.g.  
145 Gašparović, et al. 1998b). The enrichment of SAS in the SML occurs predominantly via  
146 advective and diffusive transport at low wind speeds or bubble scavenging at moderate to high  
147 wind speeds (Wurl, et al. 2011). When transferred to the atmosphere, OM with surfactant  
148 properties, ubiquitously present in atmospheric aerosol particles, has the potential to affect the  
149 cloud droplet formation ability of these particles (e.g. Kroflič, et al. 2018).

150 Sticky and gel-like TEP are secreted by phytoplankton and bacteria and can form via abiotic  
151 processes (Wurl, et al. 2009). Depending on their buoyancy they may contribute to sinking  
152 particles (marine snow) or can rise and accumulate at the sea surface. Due to their sticky nature  
153 TEP is called the “marine glue” and as such it contributes to the formation of hydrophobic films  
154 by trapping other particulate and dissolved organic compounds (Wurl, et al. 2016).  
155 Additionally, TEP is suspected to play a pivotal role in the release of marine particles into the  
156 air via sea spray and bursting bubbles (Bigg and Leck 2008).

157 Many studies recognize a possible link between marine biological activity and marine-derived  
158 organic aerosol particles (Facchini, et al. 2008; O'Dowd, et al. 2004; Ovadnevaite, et al. 2011),  
159 and thus to the SML due to the linkages outlined before. Yet, the environmental drivers and  
160 mechanisms for the OM enrichment are not very clear (Brooks and Thornton 2018; Gantt and  
161 Meskhidze 2013) and individual compound studies can only explain a small part of OM (e.g.  
162 van Pinxteren, et al. 2017; van Pinxteren and Herrmann 2013). The molecular understanding of  
163 the occurrence and the processing of OM in all marine compartments is essential for a deeper  
164 understanding and for an evidence-based implementation of organic aerosol particles and their  
165 relations to the oceans in coupled ocean-atmosphere models. Synergistic measurements in  
166 comprehensive interdisciplinary field campaigns in representative areas of the ocean and also  
167 laboratory studies under controlled conditions are required to explore the biology, physics and  
168 chemistry in all marine compartments (e.g. Quinn, et al. 2015).

169 Accordingly, the project MarParCloud together with contributions from the project MARSU  
170 addresses central aspects of ocean atmosphere interactions focusing on the marine OM within  
171 an interdisciplinary field campaign at the Cape Verde Islands. Synergistic measurements will  
172 deliver an improved understanding of the role of marine organic matter. MarParCloud focuses  
173 on the following main research questions:



- 174 • To what extent is seawater a source of OM on aerosol particles and cloud water?  
175  
176 • What are the important OM groups in oceanic surface films, aerosol particles and  
177 cloud water (and how are they linked)?  
178  
179 • Is the occurrence and accumulation of OM in the surface film and in other marine  
180 compartments (aerosol particles, cloud water) controlled by biological and  
181 meteorological factors?  
182  
183 • Which functional role do bacteria play in aerosol particles?  
184  
185 • Does the surface film contribute to the formation of ice nuclei, and at what  
186 temperatures do these nuclei become ice-active? Are these ice nuclei found in cloud  
187 water?  
188  
189 • Is the marine OM connected to the CCN concentration in the MBL?  
190  
191 • How must an emission parameterization for OM (including individual species) be  
192 designed in order to best reflect the concentrations in the aerosol depending on those  
193 in seawater or biological productivity under given ambient conditions?  
194

195 The tropics with a high photochemical activity are of central importance in several aspects of  
196 the climate system. Approximately 75% of the tropospheric production and loss of ozone occurs  
197 within the tropics, and in particular in the tropical upper troposphere (Horowitz, et al. 2003).  
198 The Cape Verde islands are located downwind of the Mauritanian coastal upwelling region off  
199 northwest in the islands. In addition, they are in a region of the Atlantic that is regularly  
200 impacted by dust deposition from the African Sahara (Carpenter, et al. 2010). The remote  
201 station of CVAO is therefore an excellent site for process-oriented campaigns embedded into  
202 the long-term measurements of atmospheric constituents, which are essential for understanding  
203 the atmospheric processes and its impact on climate.

204

## 205 2 Strategy of the campaign

206

207 The present contribution intends to provide an introduction, overview and first results of the  
208 comprehensive MarParCloud field campaign to the MarParCloud Special Issue. We will  
209 describe the oceanic and atmospheric ambient conditions at the CVAO site that have not been  
210 synthesized elsewhere and are valuable in themselves because of the sparseness of the existing  
211 information at such a tropical remote location. Next, we will describe the sampling and  
212 analytical strategy during MarParCloud, taking into account all marine compartments i.e. the  
213 seawater (SML and bulk water), ambient aerosol particles (at ground-level and the Mt Verde,  
214 elevation: 744 m a.s.l.), and cloud water. Detailed aerosol investigations were carried out, both  
215 for the chemical composition and for physical properties at both stations. In addition, vertical  
216 profiles of meteorological parameters were measured at CVAO using a helikite. These  
217 measurements were combined with modelling studies to determine the MBL height. In  
218 conjunction, they are an indicator for the mixing state within the MBL providing further



219 confidence for ground-level measured aerosol properties being representative for those at cloud  
220 level. The chemical characterization of OM in the aerosol particles as well as in the surface  
221 ocean and cloud water included sum parameters (e.g. OM classes like biopolymers and humic-  
222 like substances) and molecular analyses (e.g. lipids, sugars and amino acids). Additionally, to  
223 address the direct oceanic transfer (bubble bursting), seawater and aerosol particle  
224 characterization obtained from a systematic plunging waterfall tank are presented. As an  
225 example for trace metals, ocean surface mercury (Hg) associated with OM was studied. Marine  
226 pigments and marine microorganisms were captured to investigate their relation to OM and to  
227 algae produced trace gases. Marine trace gases such as dimethyl sulphide (DMS), VOCs and  
228 oxygenated (O)VOCs were measured and discussed. Furthermore, a series of continuous  
229 nitrous acid (HONO) measurements was conducted at the CVAO with the aim of elucidating  
230 the possible contribution of marine surfaces at the production of this acid. To explore whether  
231 marine air masses exhibit a significant potential to form SOA, an oxidation flow reactor (OFR)  
232 was deployed at the CVAO. Finally, modelling studies to describe the vertical transport of  
233 selected marine organic compounds from the ocean to the atmosphere up to cloud level taking  
234 into account advection and wind conditions will be applied. From the obtained results of organic  
235 compound measurements, a new source function for the oceanic emission of OM will be  
236 developed. The measurements, first interpretations and conclusions aggregated here will  
237 provide a basis for upcoming detailed analysis.

238

### 239 3 Experimental

240

#### 241 3.1 General CVAO site and meteorology

242

243 The Cape Verde archipelago Islands are situated in the Eastern Tropical North Atlantic  
244 (ETNA). The Archipelago experiences strong North-East trade winds that divide the islands  
245 into two groups, the Barlavento (windward) and Sotavento (leeward) islands. The North-  
246 Western Barlavento Islands of São Vicente and Santo Antão, as well as São Nicolao, are rocky  
247 and hilly making them favourable for the formation of orographic clouds.

248 The CVAO is part of a bilateral initiative between Germany and the UK to conduct long-term  
249 studies in the tropical north-east Atlantic Ocean (16° 51.49' N, -24° 52.02' E). The station is  
250 located directly at the shoreline at the northeastern tip of the island of São Vicente at 10 m a.s.l.  
251 The air temperature varies between 20 and 30 °C with a mean of 23.6 °C. The relative humidity  
252 is in average at 79% and precipitation is very low (Carpenter, et al. 2010). Due to the trade  
253 winds, this site is free from local island pollution and provides reference conditions for studies  
254 of ocean-atmosphere interactions. However, it also lies within the Saharan dust outflow corridor  
255 to the Atlantic Ocean and experiences strong seasonal dust outbreaks with peaks between late  
256 November and February (Fomba, et al. 2014; Patey, et al. 2015; Schepanski, et al. 2009). Air  
257 mass inflow to this region can vary frequently within a day leading to strong inter-day temporal  
258 variation in the aerosol mass and chemical composition (Fomba, et al. 2014, Patey, et al. 2015).



259 Despite the predominant NE trade winds, air masses from the USA as well as from Europe are  
260 partly observed. However, during autumn, marine air masses are mainly present with few  
261 periods of dust outbreaks because at these times the dust is transported at higher altitudes in the  
262 Saharan Air Layer (SAL) over the Atlantic to the Americas (Fomba, et al. 2014). During  
263 autumn, there is no significant transport of the dust at lower altitudes and only intermittent  
264 effects of turbulence in the SAL leads to occasional dust deposition and sedimentation from the  
265 SAL to lower altitudes and at ground level. Furthermore, during autumn the mountain site (Mt.  
266 Verde) is often covered with clouds as surface temperatures drop after typically very hot  
267 summer months. Due to the frequent cloud coverage and less dust influence in autumn, the  
268 MarParCloud campaign was scheduled from September 13<sup>th</sup> to October 13<sup>th</sup> 2017.

269

### 270 3.2 CVAO equipment during MarParCloud

271

272 The setup of the CVAO station is explained in detail in Carpenter, et al. (2010) and Fomba, et  
273 al. (2014). During the MarParCloud campaign, the 30 m high tower was equipped with several  
274 aerosol particle samplers, including high volume PM<sub>1</sub>, PM<sub>10</sub> (Digitel, Riemer, Germany), and  
275 total suspended particle (TSP, Sieria Anderson, USA) samplers, low volume TSP (homebuilt)  
276 and PM<sub>1</sub> (Comde-Derenda, Germany) samplers and a size-resolved aerosol particle Berner  
277 impactor (5 stages). The sampling times were usually set to 24 h (more details in the SI). On-  
278 line aerosol instruments included a Cloud Condensation Nuclei counter (CCNc, Droplet  
279 Measurement Technologies, Boulder, USA) (Roberts and Nenes 2005) to measure cloud  
280 condensation nuclei number concentration (N<sub>CCN</sub>). A TROPOS-type Scanning Mobility  
281 Particle Sizer (SMPS) (Wiedensohler, et al. 2012), and an APS (Aerodynamic Particle Sizer,  
282 model 3321, TSI Inc., Paul, MN, USA) were used to measure in the size range from 10 nm to  
283 10 μm. The particles hygroscopicity (expressed as κ (Petters and Kreidenweis 2007)) was  
284 derived from combined N<sub>CCN</sub> and particle number size distributions (PNSDs) measurements  
285 from the SMPS and APS. Vertical profiles of meteorological parameters were measured using  
286 a 16 m<sup>3</sup> Helikite (Allsopp Helikites Ltd, Hampshire, UK), a combination of a kite and a tethered  
287 balloon. Additional equipment at the CVAO station on ground included the plunging waterfall  
288 tank, the LOng Path Absorption Photometer (LOPAP), and the Gothenburg Potential Aerosol  
289 Mass Reactor (Go:PAM) chamber. Further details on the measurements are listed and explained  
290 in the SI and all instruments can be found in the Table S1.

291

292

### 293 3.3 Mt. Verde

294 Mt. Verde was a twin site for aerosol particle measurements and the only site with cloud water-  
295 sampling during the MarParCloud campaign. It is the highest point of the São Vicente Island  
296 (744 m) situated in the northeast of the Island (16° 86.95' N, -24° 93.38' E) and northwest to  
297 the CVAO. Mt. Verde also experiences direct trade winds from the ocean with no significant  
298 influence of anthropogenic activities from the island. Mt. Verde was in clouds during roughly  
299 58% of the time during the campaign. However, the duration of the cloud coverage varied  
300 between 2 h and 18 h with longer periods of cloud coverage observed in the nights when surface  
301 temperatures dropped.



302 During the campaign, Mt. Verde was, for the first time, equipped with similar collectors as  
303 operated at the CVAO, namely the high volume Digital sampler for the PM<sub>1</sub> and PM<sub>10</sub> bulk  
304 aerosol particles, a low volume TSP sampler and a five-stage Berner impactor for the size-  
305 resolved aerosol particle sampling. Bulk cloud water was collected using six (4 plastic and 2  
306 stainless steel) compact Caltech Active Strand Cloud water Collectors (CASCC2) (Demoz, et  
307 al. 1996). The six samplers were run in parallel for a sampling time between 2.5 and 13 hours  
308 collecting between 78 to 544 mL cloud water per sampler in an acid-precleared plastic bottle.  
309 It needs to be pointed out that the aerosol particle samplers run continuously and aerosol  
310 particles were also sampled during cloud events. The cloud liquid water content was measured  
311 continuously by a particle volume monitor (PVM-100, Gerber Scientific, USA), which was  
312 mounted on a support at the same height with the cloud water samplers. The same suite of on-  
313 line aerosol instruments as employed at the CVAO (SMPS, APS, CCNc) was installed at the  
314 mountain side. All instruments employed at the Mt. Verde site are listed in the Table S2.

315

#### 316 3.4 Oceanographic setting and seawater sampling site

317

318 The ETNA around Cape Verde is characterized by a so-called oxygen minimum zone (OMZ)  
319 at a water depth of approximately 450 m and by sluggish water velocities (Brandt, et al. 2015).  
320 The region is bounded by a highly productive eastern-boundary upwelling system (EBUS)  
321 along the African coast, by the Cape Verde Frontal Zone (CVFZ) on its western side, and by  
322 zonal current bands towards the equator (Stramma, et al. 2005). Upper water masses towards  
323 the archipelago are dominated by North Atlantic Central Water masses (NACW) with enhanced  
324 salinity, whereas the South Atlantic Central Water mass (SACW) is the dominating upper layer  
325 water mass in the EBUS region (Pastor, et al. 2008). Filaments and eddies generated in the  
326 EBUS region are propagating westwards into the open ocean and usually dissipate before  
327 reaching the archipelago. However, observations from the Cape Verde Ocean Observatory  
328 (CVOO) 60 nautical miles northeast of the Sao Vicente island (17° 35.00 N', -24° 17.00 E',  
329 <http://cvoos.geomar.de>) also revealed the occurrence of water masses originating from the EBUS  
330 region which got advected by stable mesoscale eddies (Fiedler, et al. 2016; Karstensen, et al.  
331 2015).

332 For the MarParCloud campaign, the water samples were taken at Bahia das Gatas, a beach that  
333 is situated upwind of the CVAO about 4 km northwest in front of the station. The beach  
334 provided shallow access to the ocean that allowed the employment of the fishing boats for  
335 manual SML and bulk water sampling and the other equipment. For SML sampling, the glass  
336 plate technique as one typical SML sampling strategy was applied (Cunliffe and Wurl 2014).  
337 A glass plate with a sampling area of 2000 cm<sup>2</sup> was vertically immersed into the water and then  
338 slowly drawn upwards with a withdrawal rate between 5 and 10 cm s<sup>-1</sup>. The surface film adheres  
339 to the surface of the glass and is removed using framed Teflon wipers (Stolle, et al. 2010; van  
340 Pinxteren, et al. 2012). Bulk seawater was collected from a depth of 1 m using a specially  
341 designed device consisting of a glass bottle mounted on a telescopic rod used to monitor  
342 sampling depth. The bottle was opened underwater at the intended sampling depth with a  
343 specifically conceived seal-opener.

344 In addition, the MarParCat, a remotely controllable catamaran, was applied for SML sampling  
345 using the same principle as manual sampling (glass plate). The MarParCat sampled bulk water



346 in a depth of 70 cm. A more detailed description of the MarParCat can be found in the SI. Using  
347 the two devices, manual sampling and the MarParCat, between one and six liters of SML were  
348 sampled at each sampling event. For the sampling of the SML, great care was taken that all  
349 parts that were in contact with the sample (glass plate, bottles, catamaran tubing) underwent an  
350 intense cleaning with 10% HCl to avoid contamination and carry over problems.  
351 The sampling sites with the different set up and equipment are illustrated in Figure 1. All  
352 obtained SML and bulk water samples and their standard parameters are listed in Table S3.

## 353 4 Ambient conditions

### 354 4.1 Atmospheric conditions during the campaign

355

#### 356 4.1.1 Marine and dust influences

357

358 During autumn, marine background air masses are mainly observed at the CVAO, interrupted  
359 by a few periods of dust outbreaks (Carpenter, et al. 2010; Fomba, et al. 2014). A 5 years'  
360 average dust record showed low concentrations with average values of  $25 \mu\text{g m}^{-3}$  and  $17 \mu\text{g m}^{-3}$   
361 during September and October, respectively (Fomba, et al. 2014). The dust concentrations  
362 during the campaign were generally  $< 30 \mu\text{g m}^{-3}$  however, strong temporal variation of mineral  
363 dust markers were observed (Table 1). According to Fomba, et al. (2013, 2014), a classification  
364 into: marine conditions (dust  $< 5 \mu\text{g/m}^3$ , typically Fe  $< 50 \text{ ng m}^{-3}$ ), low dust (dust  $< 20 \mu\text{g/m}^3$ )  
365 and moderate dust (dust  $< 60 \mu\text{g/m}^3$ ) conditions was used to describe the dust influence during  
366 this period. Following this classification, one purely marine period was defined from September  
367 22<sup>nd</sup> to 24<sup>th</sup>, which was also evident from the course of the back trajectories (Fig S11). For the  
368 other periods, the air masses were classified as mixed with marine and low or moderate dust  
369 influences as listed in Table 1. Based on a three-modal parameterization method that regarded  
370 the number concentrations in different aerosol particle modes, a similar but much finer  
371 classification of the aerosol particles was obtained as discussed in Gong, et al. (2019a).

372 The classification of the air masses was complemented by air mass backward trajectory  
373 analyses. 96 hours back trajectories were calculated on an hourly basis within the sampling  
374 intervals, using the HYSPLIT model (HYbrid Single-Particle Lagrangian Integrated Trajectory,  
375 <http://www.arl.noaa.gov/ready/hysplit4.html>, 26.07.19) published by the National Oceanic and  
376 Atmospheric Administration (NOAA) in the ensemble mode at an arrival height of  $500 \text{ m} \pm$   
377  $200 \text{ m}$  (van Pinxteren, et al. 2010). The back trajectories for the individual days of the entire  
378 campaign, based on the sampling interval for aerosol particle sampling, were calculated and are  
379 listed in Figure S11. Air parcel residence times over different sectors are plotted in Figure 2.  
380 The comparison of dust concentration and the residence time of the back trajectories revealed  
381 that in some cases low dust contributions were observed although the air masses travelled  
382 almost completely over the ocean (e.g. first days of October). In such cases, entrainment of dust  
383 from higher altitudes might explain this finding. The related transport of Saharan dust to the  
384 Atlantic during the measurement period can be seen in a visualization based on satellite  
385 observations (<https://svs.gsfc.nasa.gov/12772>, last visited on Oct. 1<sup>st</sup>, 2019). For specific days  
386 with a low MBL height, it might be more precise to employ back trajectories that start at a lower  
387 height and therefore exclude entrainment effects from the free troposphere for the



388 characterisation of CVAO data. Similarly, for investigating long-lived components, it might be  
389 helpful to analyse longer trajectory integration times (e.g. 10 days instead of 4 days). However,  
390 the longer the back trajectories, the higher is the level of uncertainty. Regarding aerosol  
391 analysis, it is important to notice that dust influences are generally more pronounced on super-  
392 micron particles than on sub-micron particles (e.g. Fomba, et al. 2013; Müller, et al. 2009;  
393 Müller, et al. 2010) meaning that bigger particles may be affected by dust sources whereas  
394 smaller particles may have stronger oceanic and anthropogenic as well as long-range transport  
395 influences. Consequently, the herein presented classification represents a first general  
396 characterisation of the air mass origins. Depending on the sampling periods of other specific  
397 analysis, slight variations may be observed and this will be indicated in the specific analysis  
398 and manuscripts.

399

#### 400 4.1.2 Meteorological condition

401

402 Air temperature, wind direction, wind speed measured between September 15<sup>th</sup> and October 6<sup>th</sup>  
403 (17.5 m a.s.l.) are shown in Figure 3 together with the mixing ratios of the trace gases ozone,  
404 ethane, ethene, acetone, methanol and DMS. During this period the air temperature ranged from  
405 25.6 °C (6:00 UTC) to 28.3 °C (14:00 UTC) with an average diurnal variation of 0.6 °C. The  
406 wind direction was north-easterly (30 to 60 °), except for a period between September 19<sup>th</sup> and  
407 20<sup>th</sup> and again on September 21<sup>st</sup> when northerly air, and lower wind speeds, prevailed. The  
408 meteorological conditions observed during the campaign were typical for this site (e.g.  
409 Carpenter, et al. 2010, Fomba, et al. 2014). The concentrations of the different trace gases will  
410 be more thoroughly discussed in section 5.3.

#### 411 4.1.3 Measured and modelled marine boundary layer (MBL) height

412

413 The characterization of the MBL is important for the interpretation of both the ground-based as  
414 well as the vertically-resolved measurements, because the MBL mixing state allows to elucidate  
415 the possible connections between ground-based processes (e.g. aerosol formation) and the  
416 higher (e.g. mountain and cloud level) altitudes. The Cape Verdes typically exhibit a strong  
417 inversion layer with a sharp increase in the potential temperature and a sharp decrease of the  
418 humidity (Carpenter, et al. 2010).

419 The vertical measurements of meteorological parameters were carried out at CVAO with a 16  
420 m<sup>3</sup> Helikite. The measurements demonstrate that a Helikite is a reliable and useful instrument  
421 that can be deployed under prevailing wind conditions such as at this measurement site. 19  
422 profiles on ten different days could be obtained and Figure 4 shows an exemplary profile, from  
423 September 17<sup>th</sup>. During the campaign, the wind speed varied between 2 and 14 m s<sup>-1</sup> and the  
424 MBL height was found to be between about 600 and 1100 m (compare to Fig. 5). Based on the  
425 measured vertical profiles, the MBL was found to be often well mixed. However, there are  
426 indications for a decoupled boundary layer in a few cases that will be further analysed.

427 As it was not possible to obtain information of the MBL height for the entire campaign from  
428 online measurements, the MBL height was also simulated using the Bulk-Richardson number.  
429 The simulations showed that the MBL height was situated where the Bulk-Richardson number



430 exceeded the critical value 0.25. Figure 5 shows, that the simulated MBL height was always  
431 lower compared to the measured one during the campaign and also compared to previous  
432 measurements reported in the literature. Based on long-term measurements, Carpenter, et al.  
433 (2010) observed an MBL height of  $713 \pm 213$  m at the Cape Verdes. In the present study a  
434 simulated MBL height of  $452 \pm 184$  m was found, however covering solely a period over one  
435 month. The differences might be caused by the grid structure of the applied model (more details  
436 in the SI). The vertical resolution of 100 to 200 m might lead to a misplacement of the exact  
437 position of the MBL-height. Moreover, the model calculations were constructed to identify the  
438 lowest inversion layer. Therefore, the modelled MBL height might represent a low, weak  
439 internal layer within the MBL and not the actual MBL. These issues will be further analysed.

440

#### 441 4.1.4 Cloud conditions

442

443 The Cape Verde Islands are dominated by a marine tropical climate and as mentioned above,  
444 marine air is constantly supplied from a north-easterly direction which also transports marine  
445 boundary-layer clouds towards the islands. Average wind profiles derived from the European  
446 Center for Medium-Range Weather Forecasts (ECWMF) model simulations are shown in  
447 Figure 6a. On the basis of the wind profiles, different cloud scenes have been selected and  
448 quantified (Derrien and Le Gleau 2005) using geostationary Meteosat SEVIRI data with a  
449 spatial resolution of 3 km (Schmetz, et al. 2002) and are shown in Figure 6b – f. The island Sao  
450 Vicente is located in the middle of each picture. The first scene at 10:00 UTC on September  
451 19<sup>th</sup> was characterized by low wind speeds throughout the atmospheric column (Fig. 6b). In this  
452 calm situation, a compact patch of low-level clouds was located north-west of the Cape Verde  
453 Islands. The cloud field was rather spatially homogeneous, i.e. marine stratocumulus, which  
454 transitioned to more broken cumulus clouds towards the island. South-eastwards of the islands,  
455 high-level ice clouds dominated and possibly mask lower-level clouds. For the second cloud  
456 scene at 10:00 UTC on September 22<sup>nd</sup> (Fig. 6c), wind speed was higher with more than  $12 \text{ m s}^{-1}$   
457 in the boundary layer. Similarly, coverage of low- to very low-level clouds was rather high  
458 in the region around Cape Verde Islands. A compact stratocumulus cloud field approached the  
459 islands from north-easterly direction. The clouds that had formed over the ocean dissolved when  
460 the flow traverses the islands. Pronounced lee effects appeared downstream of the islands.  
461 Cloud scene three at 10:00 UTC on September 27<sup>th</sup> was again during a calm phase with wind  
462 speed of a few  $\text{m s}^{-1}$  only (Fig. 6d). The scene was dominated by fractional clouds (with a  
463 significant part of the spatial variability close to or below the sensor resolution). These clouds  
464 formed locally and grew. Advection of clouds towards islands was limited. The last two cloud  
465 scenes (at 10:00 UTC on October 1<sup>st</sup> in Fig. 6e and at 10:00 UTC on October 11<sup>th</sup> in Fig. 6f)  
466 were shaped by higher boundary-layer winds and changing wind directions in higher  
467 atmospheric levels. The scene in Fig. 6e shows a complex mixture of low-level cloud fields and  
468 higher-level cirrus patches. The scene in Fig. 6f was again dominated by low- to very low-level  
469 clouds. The eastern part of the islands was embedded in a rather homogeneous stratocumulus  
470 field. A transition of the spatial structure of the cloud field happened in the centre of the domain  
471 with more cumuliform clouds and cloud clumps west to the Cape Verde Island. Overall, the  
472 majority of low-level clouds over the islands were formed over the ocean and ocean-derived  
473 aerosol particles, e.g. sea salt and marine biogenic compounds, might be expected to have some



474 influence on cloud formation. Infrequent instances of locally formed clouds influenced by the  
475 orography of the islands could be also identified in the satellite data. However, the rather coarse  
476 horizontal resolution of the satellite sensor and the missing information about time-resolved  
477 vertical profiles of thermodynamics and cloud condensate limits a further detailed  
478 characterization of these low-level cloud fields and their formation processes. A synergistic  
479 combination with ground-based in-situ and remote sensing measurements would be highly  
480 beneficial for future investigations.

#### 481 4.2 Biological seawater conditions

##### 482 4.2.1 Pigment concentration in seawater

483

484 To characterize the biological conditions at CVAO, a variety of pigments including  
485 chlorophyll-*a* (chl-*a*) were measured in the samples of Cape Verdean bulk water (data in Table  
486 S4 and illustrated in section 5.4.1). Chl-*a* is the most prominently used tracer for biomass in  
487 seawater; however information of phytoplankton composition can only be determined by also  
488 determining marker pigments. Therefore, each time when a water sample was taken, also  
489 several liters of bulk water were collected for pigment analysis (more details in the SI).  
490 Phytoplankton biomass expressed in chl-*a* was very low with  $0.11 \mu\text{g L}^{-1}$  at the beginning.  
491 Throughout the campaign two slight increases of biomass occurred, but were always followed  
492 by a biomass depression. The biomass increase occurred towards the end of the study, where  
493 pre-bloom conditions were reached with values up to  $0.6 \mu\text{g L}^{-1}$ . These are above the typical  
494 chl-*a* concentration in this area. In contrast, the abundance of chlorophyll degradation products  
495 as phaeophorbide *a* and phaeophythin *a* decreased over time. The low concentrations of the  
496 chlorophyll degradation products suggested that only moderate grazing took place and the  
497 pigment-containing organisms were fresh and in a healthy state. The most prominent pigment  
498 throughout the campaign was zeaxanthin, suggesting *cyanobacteria* being the dominant group  
499 in this region. This is in a good agreement with the general low biomass in the waters of the  
500 Cape Verde region and in line with previous studies, reporting the dominance of cyanobacteria  
501 during the spring and summer seasons (Franklin, et al. 2009; Hepach, et al. 2014; Zindler, et al.  
502 2012). However, once the biomass increased, *cyanobacteria* were repressed by *diatoms* as  
503 indicated by the relative increase of fucoxanthin. The *prymnesiophyte* and *haptophyte* marker  
504 19-hexanoyloxyfucoxanthin and the *pelagophyte* and *haptophytes* marker 19-  
505 butanoyloxyfucoxanthin were present and also increased when *cyanobacteria* decreased. In  
506 contrast, *dinoflagellates* and *chlorophytes* were background communities as indicated by their  
507 respective markers peridinin and chlorophyll b. Still, *chlorophytes* were much more abundant  
508 than *dinoflagellates*. In summary, the pigment composition indicated the presence of  
509 *cyanobacteria*, *haptophytes* and *diatoms* with a change in dominating taxa (from *cyanobacteria*  
510 to *diatoms*). The increasing concentration of chl-*a* and fucoxanthin implied that a bloom started  
511 to develop within the campaign dominated by *diatoms*. The increasing concentrations could  
512 also be related to changing water masses, however, since the oceanographic setting was  
513 relatively stable, the increasing chl-*a* concentrations suggest that a local bloom had developed,  
514 that might be related to the low but permanent presence of atmospheric dust input, which needs  
515 further verification. In the course of further data analysis of the campaign, the phytoplankton  
516 groups will be related to the abundance of e.g. DMS (produced by *haptophytes*) or isoprene that



517 has been reported to be produced by *diatoms* or *cyanobacteria* (Bonsang , et al. 2010), as well  
518 as to other VOCs.

#### 519 4.2.2 Wave glider fluorescence measurements

520

521 Roughly at the same time as the MarParCloud field campaign took place, an unmanned surface  
522 vehicle (SV2 Wave Glider, Liquid Robotics Inc.) equipped with a biogeochemical sensor  
523 package, a conductivity-temperature-depth sensor (CTD) and a weather station was operated in  
524 the vicinity of the sampling location. The Wave Glider carried out continuous measurements of  
525 surface water properties (water intake depth: 0.3 m) along a route near the coast (Fig. 7a), and  
526 on October 5<sup>th</sup> it was sent on a transect from close to the sampling location towards the open  
527 ocean in order to measure lateral gradients in oceanographic surface conditions.

528 The glider measurements delivered information on the spatial resolution of several parameters.  
529 Fluorescence measurements, which can be seen as a proxy of chl-*a* concentration in surface  
530 waters and hence of biological production, indicated some enhanced production leeward of the  
531 islands and also at one location upwind of the island of Santa Luzia next to São Vicente. In the  
532 vicinity of the MarParCloud sampling site the glider observed a slight enhancement in  
533 fluorescence when compared to open-ocean waters. This is in agreement with the measured  
534 pigment concentration. The overall pattern of slightly enhanced biological activity was also  
535 confirmed by satellite fluorescence measurements (Fig. 7b). However, both in situ glider and  
536 sample data as well as remote sensing data did not show any particular strong coastal bloom  
537 events and thus indicate that the MarParCloud sampling site well represented the open-ocean  
538 regime during the sampling period.

539

## 540 5 Measurements and selected results

541

### 542 5.1 Vertical resolution measurements

543

#### 544 5.1.1 Physical aerosol characterization

545

546 Based on aerosol particles measured during the campaign, air masses could be classified into  
547 different types, depending on differences in PNSDs. Marine type and dust type air masses could  
548 be clearly distinguished, even if the measured dust concentrations were only low to medium,  
549 according to the annual mean at the CVAO (Fomba, et al. 2013, 2014). The median of PNSDs  
550 during marine conditions is illustrated in Figure 8 and showed three modes, i.e., Aitken,  
551 accumulation and coarse mode. There was a minimum between the Aitken- and accumulation-  
552 mode of PNSDs (Hoppel minimum; see (Hoppel, et al. 1986) at roughly 70 nm. PNSDs  
553 measured during marine type air masses featured the lowest Aitken, accumulation and coarse  
554 mode particle number concentrations, with median values of 189, 143 and 7 cm<sup>-3</sup>, respectively.  
555 The PNSDs present during times with dust influences featured a single mode in the sub-micron  
556 size range (Fig. 8), and no visible Hoppel minimum was found. The dust type air masses  
557 featured the highest total particle number concentration (994 cm<sup>-3</sup>) and a median coarse-mode



558 particle number concentration of  $44 \text{ cm}^{-3}$ . The particle number concentrations for the coarse  
559 mode of the aerosol particles that is attributed to sea spray aerosol (SSA) accounted for about  
560 3.7% of  $N_{\text{CCN}, 0.30\%}$  (CCN number concentration at 0.30% supersaturation) and for 1.1% to 4.4%  
561 of  $N_{\text{total}}$  (total particle number concentration). A thorough statistical analysis of  $N_{\text{CCN}}$  and  
562 particle hygroscopicity concerning different aerosol types is reported in Gong, et al. (2019a).  
563 Figure 9a shows the median of marine type PNSDs for cloud free conditions and cloud events  
564 at CVAO and Mt. Verde. Figure 9b shows the scatter plot of  $N_{\text{CCN}}$  at CVAO versus those on  
565 Mt. Verde. For cloud free conditions, all data points are close to the 1:1 line, indicating  $N_{\text{CCN}}$   
566 being similar at the CVAO and Mt. Verde. However, during cloud events, larger particles,  
567 mainly accumulation- and coarse-mode particles, were activated to cloud droplet and were,  
568 consequently, removed by the inlet. Therefore,  $N_{\text{CCN}}$  at the CVAO was larger than those on Mt.  
569 Verde. Altogether, these measurements suggested that, for cloud free conditions, the aerosol  
570 particles measured at ground level (CVAO) represent the aerosol particles at the cloud level  
571 (Mt. Verde).  
572

#### 573 5.1.2 Chemical composition of aerosol particles and cloud water

574  
575 Between October 2<sup>nd</sup> and 9<sup>th</sup>, size-resolved aerosol particles at the CVAO and the Mt. Verde  
576 were collected simultaneously. The relative contribution of their main chemical constituents  
577 (inorganic ions, water-soluble organic matter (WSOM), and elemental carbon) at both sites is  
578 shown in Figure 10. Sulfate, ammonium, and WSOM dominated the sub-micron particles. The  
579 super-micron particles were mainly composed of sodium and chloride at both stations. These  
580 findings agreed well with previous studies at the CVAO (Fomba, et al. 2014; van Pinxteren, et  
581 al. 2017). The absolute concentrations of the aerosol constituents were lower at the Mt. Verde  
582 compared to the CVAO site (Table S5); they were reduced by factor of seven (super-micron  
583 particle) and by a factor of four (sub-micron particles). This decrease in the aerosol mass  
584 concentrations and the differences in chemical composition between the ground-based aerosol  
585 particles and the ones at Mt. Verde, could be due to cloud effects as described in the previous  
586 section. Different types of clouds consistently formed and disappeared during the sampling  
587 period of the aerosol particles at the Mt. Verde (more details about the frequency of the cloud  
588 events are available in the SI and in Gong, et al., (2019a) and potentially affected the aerosol  
589 chemical composition. These effects will be more thoroughly examined in further analysis.  
590 A first insight in the cloud water composition of a connected cloud water sampling event from  
591 October 5<sup>th</sup> till October 6<sup>th</sup> is presented in Figure 11. Sea salt, sulfate and nitrate compounds  
592 dominated the chemical composition making up more than 90% of the mass of the investigated  
593 chemical constituents. These compounds were also observed in the coarse fraction of the  
594 aerosol particles, indicating that the coarse mode particles served as efficient CCN and were  
595 efficiently transferred to the cloud water. No strong variations were found for the main cloud  
596 water constituents over the here reported sampling period. However, the WSOM contributed  
597 with maximal 10% to the cloud water composition and with higher contributions in the  
598 beginning and at the end of the sampling event, which warrants further analysis. The measured  
599 pH values of the cloud water samples ranged between 6.3 and 6.6 and are in agreement with  
600 literature data for marine clouds (Herrmann, et al. 2015). In summary, cloud water chemical  
601 composition seemed to be controlled by coarse mode aerosol particle composition, and the



602 presence of inorganic marine tracers (sodium, methane sulfonic acid) strongly suggested an  
603 oceanic influence on cloud water.

604

## 605 5.2 Lipid biomarkers in aerosol particles

606 Lipids from terrestrial sources such as plant waxes, soils and biomass burning have frequently  
607 been observed in the remote marine troposphere (Kawamura, et al. 2003; Simoneit, et al. 1977)  
608 and are common in marine deep-sea sediments. Within MarParCloud, marine-derived lipids  
609 were characterized in aerosol particles using lipid biomarkers in conjunction with compound  
610 specific stable carbon isotopes. Bulk aerosol filters sampled at the CVAO and PM<sub>10</sub> filter  
611 sampled at the Mt. Verde (not reported here) were extracted and the lipids were separated into  
612 functional groups for molecular and compound specific carbon isotope analysis. The content of  
613 identifiable lipids was highly variable and ranged from 4 to 140 ng m<sup>3</sup>. These concentrations  
614 are in the typical range for marine aerosol particles (Mochida, et al. 2002; Simoneit, et al. 2004)  
615 but somewhat lower than previously reported for the tropical North East Atlantic (Marty &  
616 Saliot, 1979) and 1 to 2 orders of magnitude lower than reported from urban and terrestrial rural  
617 sites (Simoneit, 2004). It mainly comprised the homologue series of n-alkanoic acids, n-  
618 alkanols and n-alkanes. Among these the c16:0 acid and the c18:0 acids were by far the  
619 dominant compounds, each contributing 20 to 40% to the total observed lipids. Among the  
620 terpenoids, dehydroabietic acid, 7-oxo-dehydroabietic acid and friedelin were in some samples  
621 present in remarkable amounts. Other terpenoid biomarker in particular phytosterols were rarely  
622 detectable. The total identifiable lipid content was inversely related to dust concentration, as  
623 shown exemplary for the fatty acids (Fig. 12) with generally higher lipid concentrations in  
624 primary marine air masses. This is consistent with previous studies reporting low lipid yields  
625 in Saharan dust samples and higher yields in dust from the more vegetated Savannahs and dry  
626 tropics (Simoneit, et al. 1977). First measurements of typical stable carbon isotope ratios of the  
627 lipid fractions were (-28.1 ± 2.5) ‰ for the fatty acids and (-27.7 ± 0.7) ‰ for the n-alkanes  
628 suggesting a mixture of terrestrial c3 and c4, as well as marine sources. In a separate  
629 contribution the lipid fraction of the aerosol particles in conjunction with its typical stable  
630 carbon isotope ratios will be further resolved.

631

## 632 5.3 Trace gas measurements

### 633 5.3.1 Dimethyl sulphide, ozone and (oxygenated) volatile organic compounds

634

635 Trace gases such as dimethyl sulfide (DMS), volatile organic compounds (VOCs) and  
636 oxygenated (O)VOCs have been measured during the campaign and the results are presented  
637 together with the meteorological data in Figure 3. The atmospheric mixing ratios of DMS  
638 during this period ranged between 68 ppt and 460 ppt with a mean of 132 ± 57ppt (1σ). These  
639 levels were higher than the annual average mixing ratio for 2015 of 57 ± 56 ppt, however this  
640 may be due to seasonably high and variable DMS levels observed during summer and autumn  
641 at Cape Verde (observed mean mixing ratios were 86 ppt and 107 ppt in September and October  
642 2015). High DMS concentrations on September 19<sup>th</sup> – 20<sup>th</sup> occurred when air originated



643 predominantly from the Mauritanian upwelling region and on September 26<sup>th</sup> and 27<sup>th</sup> when the  
644 footprint was influenced by southern hemisphere (Figure SI1). These elevated concentrations  
645 will be linked to the phytoplankton composition reported in section 4.2.1. to elucidate  
646 associations for example between DMS and coccolith (individual plates of calcium carbonate  
647 formed by *coccolithophores* phytoplankton) as observed by Marandino, et al. (2008). Ethene  
648 showed similar variability to DMS, with coincident peaks (> 300 ppt DMS and > 40 ppt ethene)  
649 on September 20<sup>th</sup>, 26<sup>th</sup> and 27<sup>th</sup>, consistent with an oceanic source for ethene. Ethene can be  
650 emitted from phytoplankton (e.g. McKay, et al. 1996) and therefore it is possible that it  
651 originated from the same biologically active regions as DMS. In the North Atlantic atmosphere,  
652 alkenes such as ethene emitted locally have been shown to exhibit diurnal behaviour with a  
653 maximum at solar noon, suggesting photochemical production in seawater (Lewis, et al. 2005).  
654 There was only weak evidence of diurnal behaviour at Cape Verde (data not shown), possibly  
655 because of the very short atmospheric lifetime of ethene (8 hours assuming  $[OH] = 4 \times 10^6$   
656 molecules  $cm^{-3}$ , Vaughan, et al. 2012) in this tropical environment, which would mask  
657 photochemical production. Mean acetone and methanol mixing ratios were 782 ppt (566 ppt –  
658 1034 ppt) and 664 ppt (551 ppt – 780 ppt), respectively. These are similar to previous  
659 measurements at Cape Verde and in the remote Atlantic at this time of year (Lewis, et al. 2005;  
660 Read, et al. 2012). Methanol and acetone showed similar broad-scale features, indicating  
661 common sources. Highest monthly methanol and acetone concentrations have often been  
662 observed in September at Cape Verde, likely as a result of increased biogenic emissions from  
663 vegetation or plant matter decay in the Sahel region of Africa (Read, et al. 2012). In addition to  
664 biogenic sources, (O)VOCs are anthropogenically produced from fossil fuels and solvent usage  
665 in addition to having a secondary source from the oxidation of precursors such as methane.  
666 Carpenter, et al. (2010) showed that air masses originating from North America (determined  
667 via 10-day back trajectories) could impact (O)VOCs at the CVAO.  
668 The average ozone mixing ratio during the campaign was 28.7 ppb (19.4 ppb – 37.8 ppb). Lower  
669 ozone concentrations on September 27<sup>th</sup> to 28<sup>th</sup> were associated with influence from southern  
670 hemispheric air. Ozone showed daily photochemical loss, as expected in these very low-NOx  
671 conditions, on most days with an average daily (from 9:00 UTC to 17:00 UTC) loss of 4 ppbV.  
672 It was previously shown that the photochemical loss of O<sub>3</sub> at Cape Verde and over the remote  
673 ocean is attributable to halogen oxides (29% at Cape Verde) as well as ozone photolysis (54%)  
674 (e.g. Read, et al. 2008). Altogether, for the trace gases, a variety of conditions were observed  
675 in this three-week period with influence from ocean-atmosphere exchange and also potential  
676 impacts of long-range transport.

677

### 678 5.3.2 Nitrous acid

679 Nitrous acid (HONO) plays a significant role in the atmospheric chemistry as an important  
680 source of hydroxyl radical (\*OH). It is well recognized that significant uncertainties remain on  
681 its emission sources as well as on its in-situ tropospheric formation processes. During the  
682 campaign, a series of continuous measurements of HONO has been conducted, aiming at  
683 evaluating the possible contribution of marine surfaces to the production of HONO. The  
684 measurements indicated that HONO concentrations exhibited diurnal variations peaking at  
685 noontime. The concentrations during daytime (08:00 to 17:00, local time) and nighttime (17:30



686 to 07:00 local time) periods were around 20 ppt and 5 ppt on average, respectively. The fact  
687 that the observed data showed higher values during the day compared to the nighttime was quite  
688 surprising since HONO is expected to be photolyzed during the daytime. If confirmed, the  
689 measurements conducted here may indicate that there is an important HONO source in the area  
690 of interest. In a separate paper, the data obtained will be described and discussed and tentative  
691 explanation of the observed phenomena will be developed.

692

693

#### 694 5.4 Organic Matter and related compounds in seawater

695

##### 696 5.4.1. Dissolved organic carbon

697

698 Dissolved organic carbon (DOC) comprise a complex mixtures of different compound groups  
699 and is diverse in its composition. For a first overview, DOC as a sum parameter was analyzed  
700 in all SML and bulk water samples (data in Table S4). DOC concentration varied between 1.8  
701 and 3.2 mg L<sup>-1</sup> in the SML and 0.9 and 2.8 mg L<sup>-1</sup> in the bulk water and were in general  
702 agreement with previous studies at this location (e.g. van Pinxteren, et al. 2017). A slight  
703 enrichment in the SML with an enrichment factor (EF) = 1.66 (±0.65) was found, i.e. SML  
704 concentrations contain roughly 70% more DOC than the corresponding bulk water. The  
705 concentrations of DOC in the bulk water together with the temporal evolution of biological  
706 indicators (pigments and the total bacterial cell numbers) and atmospheric dust concentrations  
707 are presented in Figure 13. First analysis show that the DOC concentrations were not directly  
708 linked to the increasing chl-*a* concentrations, however their relation to single pigments, the  
709 background dust concentrations and to wind speed and solar radiation will be further resolved  
710 to elucidate potential biological and meteorological controls on the concentration and  
711 enrichment of DOC.

712 For several dates, both SML sampling devices (glass plate and catamaran) were applied in  
713 parallel to compare the efficiency of different sampling approaches: manual glass plate and the  
714 catamaran sampling (Fig. 14). As mentioned above both techniques used the same principle,  
715 i.e. the collection of the SML on a glass plate and its removal with a Teflon wiper. The deviation  
716 between both techniques concerning DOC measurements was below 25% in 17 out of 26  
717 comparisons and therefore within the range of variability of these measurements. However, in  
718 roughly 30% of all cases the concentration differences between manual glass plate and  
719 catamaran were larger than 25%. The discrepancy for the bulk water results could be related to  
720 the slightly different bulk water sampling depths using the MarParCat bulk water sampling  
721 system (70 cm) and the manual sampling with the telescopic rods (100 cm). Although the upper  
722 meters of the ocean are assumed to be well mixed, recent studies indicate that small scale  
723 variabilities can be observed already within the first 100 cm of the ocean (Robinson, et al.  
724 2019a).

725 The variations within the SML measurements could be due to the patchiness of the SML that  
726 has been tackled in previous studies (e.g. Mustafa, et al. 2017, 2018). Small-scale patchiness  
727 was recently reported as a common feature of the SML. The concentrations and compositions  
728 probably undergo more rapid changes due to a high physical and biological fluctuations.



729 Mustafa, et al. (2017) have recently shown that the enrichment of fluorescence dissolved  
730 matter (a part of DOC) showed short time-scale variability, changing by 6% within ten-minute  
731 intervals. The processes leading to the enrichment of OM in the SML are probably much more  
732 complex than previously assumed (Mustafa, et al. 2018). In addition, the changes in DOC  
733 concentrations between the glass plate and the catamaran could result from the small variations  
734 of the sampling location as the catamaran was typically 15 to 30 m apart from the boat where  
735 the manual glass plate sampling was carried out.

736 Given the high complex matrix of seawater and especially the SML, the two devices applied  
737 were in quite good agreement considering DOC measurements. However, this is not necessarily  
738 the case for the single parameters like specific organic compounds and INP concentrations.  
739 Especially low concentrated constituents might be more affected by small changes in the  
740 sampling procedure and this remains to be evaluated for the various compound classes.

741

#### 742 5.4.2. Surfactants and lipids in seawater

743

744 Due to their physicochemical properties, surfactants (SAS) are enriched in the SML relative to  
745 the bulk water and form surface films (Frka, et al. 2009; Frka, et al. 2012; Wurl, et al. 2009).  
746 During the present campaign, the SAS in the dissolved fraction of the SML samples ranged  
747 from 0.037 to 0.125 mg TX-100 eqL<sup>-1</sup> (Triton-X-100 equivalents) with a mean of 0.073 ± 0.031  
748 mg TX-100 eqL<sup>-1</sup> (n = 7). For bulk water, the dissolved SAS ranged from 0.020 to 0.068 mg  
749 TX-100 eqL<sup>-1</sup> (mean 0.051 ± 0.019 mg TX-100 eqL<sup>-1</sup>, n = 12). The SAS enrichment showed  
750 EFs from 1.01 to 3.12 (mean EF = 1.76 ± 0.74) (Fig. 15) and was slightly higher than that for  
751 the DOC (mean EF = 1.66 ± 0.65) indicating some higher surfactant activity of the overall  
752 DOM in the SML in respect to the bulk DOM. An accumulation of the total dissolved lipids  
753 (DL) in the SML was observed as well (mean EF = 1.27 ± 0.12). Significant correlation was  
754 observed between the SAS and DL concentrations in the SML (r = 0.845, n = 7, p < 0.05) while  
755 no correlation was detected for the bulk water samples. Total DL concentrations ranged from  
756 82.7 to 148 µg L<sup>-1</sup> (mean 108 ± 20.6 µg L<sup>-1</sup>, n = 8) and from 66.5 to 156 µg L<sup>-1</sup> (mean 96.9 ±  
757 21.7 µg L<sup>-1</sup>, n = 17) in the SML and the bulk water, respectively. In comparison to the bulk  
758 water, the SML samples were enriched with lipid degradation products e.g. free fatty acids and  
759 long chain alcohols (DegLip; mean EF = 1.50 ± 0.32), particularly free fatty acids and long-  
760 chain alcohols (Fig. 15), pointing to their accumulation from the bulk and/or enhanced OM  
761 degradation within the SML. DegLip are strong surface-active compounds (known as dry  
762 surfactants), which play an important role in surface film establishment (Garrett 1965). The  
763 overall surfactant activity of the SML is the result of the competitive adsorption of highly  
764 surface-active lipids and other less surface-active macromolecular compounds  
765 (polysaccharides, proteins, humic material) (Ćosović and Vojvodić 1998) dominantly present  
766 in seawater. The presence of even low amounts of lipids results in their significant contribution  
767 to the overall surface-active character of the SML complex organic mixture (Frka, et al. 2012).  
768 The observed biotic and/or abiotic lipid degradation processes within the SML will be further  
769 resolved by combining surfactant and lipid results with detailed pigment characterisation and  
770 microbial measurements. The same OM classes of the ambient aerosol particles will be  
771 investigated and compared with the seawater results. This will help to tackle the questions to



772 what extent the seawater exhibits a source of OM on aerosol particles and which important  
773 aerosol precursors are formed or converted in surface films.

774

#### 775 5.5 Seawater Untargeted Metabolomics

776 For a further OM characterization of SML and bulk seawater an ambient MS-based  
777 metabolomics method using direct analysis in real time quadrupole time-of-flight mass  
778 spectrometry (DART-QTOF-MS) coupled to multivariate statistical analysis was designed  
779 (Zabalegui, et al., 2019). A strength of a DART ionization source is that it is less affected by  
780 high salt levels than an electrospray ionization source (Kaylor, et al. 2014), allowing the  
781 analysis of seawater samples without observing salt deposition at the mass spectrometer inlet,  
782 or having additional limitations such as low ionization efficiency due to ion suppression (Tang,  
783 et al. 2004). Based on these advantages, paired SML/bulk water samples were analyzed without  
784 the need of desalinization by means of a transmission mode (TM) DART-QTOF-MS-based  
785 analytical method that was optimized to detect lipophilic compounds (Zabalegui, et al., 2019).  
786 An untargeted metabolomics approach, addressed as seaomics, was implemented for sample  
787 analysis. SML samples were successfully discriminated from ULW samples based on a panel  
788 of ionic species extracted using chemometric tools. The coupling of the DART ion source to  
789 high-resolution instrumentation allowed generating elemental formulae for unknown species  
790 and tandem MS capability contributed to the identification process. Tentative identification of  
791 discriminant species and the analysis of relative compound abundance changes among sample  
792 classes (SML and bulk water) suggested that fatty alcohols, halogenated compounds, and  
793 oxygenated boron-containing organic compounds may be involved in water-air transfer  
794 processes and in photochemical reactions at the water-air interface of the ocean (Zabalegui, et  
795 al., 2019). These identifications (e.g. fatty alcohols) agree well with the abundance of lipids in  
796 the respective samples. In this context, TM-DART-HR-MS appears to be an attractive strategy  
797 to investigate the seawater OM composition without requiring a desalinization step.

798

#### 799 5.6 Ocean surface mercury associated with organic matter

800

801 Several trace metals are known to accumulate in the SML. In the case of Hg, the air-sea  
802 exchange plays an important role in its global biogeochemical cycle and hence processing of  
803 Hg in the SML is of particular interest. Once deposited from the atmosphere to the ocean surface  
804 via dry and wet deposition, the divalent mercury ( $\text{Hg}^{\text{II}}$ ) can be transported to the deeper ocean  
805 by absorbing on sinking OM particles, followed by methylation. On the other hand,  $\text{Hg}^{\text{II}}$   
806 complexed by DOM in the ocean surface can be photo-reduced to  $\text{Hg}^0$ , which evades into the  
807 gas phase. In both processes, OM, dissolved or particulate, is the dominant factor influencing  
808 the complexation and adsorption of Hg. To explore the Hg behaviour with OM, the  
809 concentrations of total and dissolved Hg as well as the methylmercury (MeHg) were determined  
810 in the SML and in the bulk water using the US EPA method 1631 and 1630, as described in Li,  
811 et al. (2018). Figure 16 shows the concentrations of Hg and MeHg associated with DOC and  
812 POC in the SML and bulk water. The total Hg concentrations were 3.6 and 4.6  $\text{ng L}^{-1}$  in the  
813 SML but 3.1 and 1.3  $\text{ng L}^{-1}$  in the bulk water on September 26<sup>th</sup> and 27<sup>th</sup>, respectively, which  
814 were significantly enriched compared to data reported for the deep North Atlantic ( $0.18 \pm 0.06$



815 ng L<sup>-1</sup>) (Bowman, et al. 2015). Atmospheric deposition and more OM adsorbing Hg are  
816 supposed to result in the high total Hg at ocean surface. The dissolved Hg concentrations were  
817 enriched by 1.7 and 2.7 times in the SML relative to bulk water, consistent with the enrichments  
818 of DOC by a factor of 1.4 and 1.9 on September 26<sup>th</sup> and 27<sup>th</sup>, respectively. Particulate Hg in  
819 the SML accounted for only 6% of the total Hg concentration on September 26<sup>th</sup> but 55% on  
820 September 27<sup>th</sup>, in contrast to their similar fractions of ~35% in the bulk water on both days.  
821 According to the back trajectories (Figure SII) stronger contribution of African continental  
822 sources (e.g., dust) was observed on September 27<sup>th</sup> that might be linked to in the higher  
823 concentrations of particulate Hg in the SML on this day. The water-particle partition  
824 coefficients (logK<sub>d</sub>) for Hg in the SML (6.8 L kg<sup>-1</sup>) and bulk water (7.0 L kg<sup>-1</sup>) were similar  
825 regarding POC as the sorbent, but one unit higher than the reported logK<sub>d</sub> values in seawater  
826 (4.9–6.1 L kg<sup>-1</sup>) (Batrakova, et al. 2014). MeHg made up lower proportions of the total Hg  
827 concentrations in the SML (2.0%) than bulk water (3.4% and 4.2%), probably due to photo-  
828 degradation or evaporation of MeHg at the surface water (Blum, et al. 2013). From the first  
829 results, it seems that the SML is the major compartment where Hg associated with OM is  
830 enriched, while MeHg is more likely concentrated in deeper water. The limited data underlines  
831 the importance of SML in Hg enrichment dependent on OM, which needs further studies to  
832 understand the air-sea exchange of Hg.

833

## 834 5.7 Ocean-atmosphere transfer of organic matter and related compounds

835

### 836 5.7.1 Dissolved organic matter classes

837

838 To investigate the complexity of dissolved organic matter (DOM) compound groups, liquid  
839 chromatography, organic carbon detection, organic nitrogen detection, UV absorbance  
840 detection (LC-OCD-OND-UVD; Huber, et al. (2011), more details in the SI) was applied to  
841 identify five different DOM classes. These classes include (i) biopolymers (likely hydrophobic,  
842 high molecular weight >> 20.000 g mol<sup>-1</sup>, largely non-UV absorbing extracellular polymers);  
843 (ii) “humic substances” (higher molecular weight ~ 1000 g mol<sup>-1</sup>, UV absorbing); (iii) “building  
844 blocks” (lower molecular weight 300-500 g mol<sup>-1</sup>, UV absorbing humics); (iv) low molecular  
845 weight “neutrals” (350 g mol<sup>-1</sup>, hydro- or amphiphilic, non-UV absorbing); and (v) low  
846 molecular weight acids (350 g mol<sup>-1</sup>). These measurements were performed from a first set of  
847 samples from all the ambient marine compartments. That comprised three SML samples and  
848 the respective bulk water, three aerosol particle filter samples (PM<sub>10</sub>) from the CVAO and two  
849 from the Mt. Verde and finally four cloud water samples collected during the campaign. The  
850 SML EFs for DOM varied from 0.83 to 1.46, which agreed very well to the DOC measurements  
851 described in section 5.4.1. A clear compound group that drove this change could not be  
852 identified so far. Figure 17 shows the relative composition of the measured DOM groups in the  
853 distinct marine compartments as an average of the single measurements (concentrations are  
854 listed in Table S6). In the SML and in the bulk water, the low molecular weight neutral  
855 (LMWN) compounds generally dominated the overall DOM pool (37 to 51%). Humic-like  
856 substances, building blocks, and biopolymeric substances contributed 22 to 32%, 16 to 23%,  
857 and 6 to 12%, respectively. Interestingly, low molecular weight acids (LMWA) were



858 predominantly observed in the SML (2 to 8%) with only one bulk water time point showing  
859 any traces of LMWA. This finding agreed well with the presence of free amino acids (FAA) in  
860 the SML; e.g. the sample with highest LMWA concentration showed highest FAA  
861 concentration (more details in Triesch, et al., 2019). Further interconnections between the DOM  
862 fractions and single organic markers and groups (e.g. sugars, lipids and surfactants, see section  
863 5.4.2) are subject to ongoing work. In contrast, aerosol particles were dominated by building  
864 blocks (46 to 66%) and LMWN (34 to 51%) compound groups, with a minor contribution of  
865 LMWA (> 6%). Interestingly, higher molecular weight compounds of humic-like substances  
866 and biopolymers were not observed. Cloud water samples had a variable contribution of  
867 substances in the DOM pool with humic substances and building blocks generally dominating  
868 (27 to 63% and 16 to 29%, respectively) and lower contributions of biopolymers (2 to 4%) and  
869 LMW acids and neutrals (1 to 20% and 18 to 34%) observed. The first measurements indicate  
870 that the composition of the cloud waters is more consistent with the SML and bulk water and  
871 different from the aerosol particle's composition. This observation suggests a two-stage process  
872 where selective aerolisation mobilises lower molecular weight humics (building blocks) into  
873 the aerosol particle phase, which may aggregate in cloud waters to form larger humic substances  
874 in cloud waters. These preliminary observations need to be further studied with a larger set of  
875 samples and could relate to either different solubilities of the diverse OM groups in water, the  
876 interaction between DOM and particulate OM (POM), including TEP formation, as well as  
877 indicating the different OM sources and transfer pathways. In addition, the chemical conditions,  
878 like pH-value or redox, could preferentially preserve or mobilise DOM fractions within the  
879 different types of marine waters. In summary, all investigated compartments showed a  
880 dominance of LMW neutrals and building blocks, which suggests a link between the seawater,  
881 aerosol particles and cloud water at this location and possible transfer processes. Furthermore,  
882 the presence of humic-like substances and biopolymers and partly LMWA in the seawater and  
883 cloud water, but not in the aerosol particles, suggests an additional source or formation pathway  
884 of these compounds. For a comprehensive picture; however, additional samples need to be  
885 analysed and interpreted in future work. It is worth noting that the result presented here are the  
886 first for such a diverse set of marine samples and demonstrate the potential usefulness in  
887 identifying changes in the flux of DOM between marine compartments.

#### 889 5.7.2. Transparent exopolymer particles: field and tank measurements

890  
891 As part of the OM pool, gel particles, such as positive buoyant transparent exopolymer particles  
892 (TEP), formed by the aggregation of precursor material released by plankton and bacteria,  
893 accumulate at the sea surface. The coastal water in Cape Verde has shown to be oligotrophic  
894 with low chl-*a* abundance during the campaign (more details in section 4.2.1). Based on  
895 previous work (Wurl, et al. 2011) it is expected that surfactant enrichment, which is closely  
896 linked to TEP enrichment, in the SML would be higher in oligotrophic waters but have a lower  
897 absolute concentration. This compliments the here achieved findings, which showed low TEP  
898 abundance in these nearshore waters; the abundance in the bulk water ranged from 37 to 144  
899  $\mu\text{gXeqL}^{-1}$  (xanthan gum equivalents) and 99 to 337  $\mu\text{gXeqL}^{-1}$  in the SML. However while the  
900 SML layer was relatively thin ( $\sim 125 \mu\text{m}$ ) there was positive enrichment of TEP in the SML



901 with an average EF of  $2.0 \pm 0.8$  (Fig. 18a). The enrichment factor for TEP was furthermore  
902 very similar to surfactant enrichment (section 5.4.2).  
903 In addition to the field samples, a tank experiment was run simultaneously using the same  
904 source of water (Fig. 18b). Breaking waves were produced via a waterfall system (details in the  
905 SI) and samples were collected from the SML and bulk water after a wave simulation time of  
906 3 h. TEP abundance in the tank experiment matched the field samples at the beginning but  
907 quickly increased to  $1670 \mu\text{gXeql}^{-1}$  in the SML with an EF of 13.2 after the first day of  
908 bubbling. The enrichment of TEP in the SML during the tank experiment had a cyclical increase  
909 and decrease pattern. Interestingly, in the field samples, even on days with moderate wind  
910 speeds ( $> 5 \text{ m s}^{-1}$ ) and occasional presence of white caps, TEP abundance or enrichment didn't  
911 increase, but it did increase substantially due to the waves in the tank experiment. This suggests  
912 that the simulated waves are very effective in enriching TEP in the SML and TEP were more  
913 prone to transport or formation by bubbling than by other physical forces, confirming bubble-  
914 induced TEP enrichment in recent artificial set-ups (Robinson, et al. 2019b). Besides the  
915 detailed investigations of TEP in seawater, first analyses show a clear abundance of TEP in the  
916 aerosol particles and in cloud water. Interestingly, a major part of TEP seems to be located in  
917 the sub-micron aerosol particles (Fig. 19). Sub-micron aerosol particles represent the longest  
918 living aerosol particle fraction and have a high probability to reach cloud level and the  
919 occurrence of TEP in cloud water strongly underlines a possible vertical transport of these  
920 ocean-derived compounds.

### 921 5.7.3 Bacterial abundance in distinct marine samples: field and tank measurements 922

923 The OM concentration and composition is closely linked with biological and especially  
924 microbial processes within the water column. Throughout the sampling period, the temporal  
925 variability of bacterial abundance in SML and bulk water was studied (data listed in Tab.SI4).  
926 Mean absolute cell numbers were  $1.3 \pm 0.2 \times 10^6 \text{ cells mL}^{-1}$  and  $1.2 \pm 0.1 \times 10^6 \text{ cells mL}^{-1}$  for  
927 SML and bulk water, respectively (Fig. 20a, all data listed in Table S4). While comparable  
928 SML data is lacking for this oceanic province, our data is in range with previous reports for  
929 surface water of subtropical regions (Zäncker, et al. 2018). A strong day-to-day variability of  
930 absolute cell numbers was partly observed (e.g. the decline between September 25<sup>th</sup> and 26<sup>th</sup>),  
931 but all these changes were found in both, in the SML and bulk water (Fig. 20a). This indicates  
932 that the upper water column of the investigated area experienced strong changes, e.g. by inflow  
933 of different water masses and/or altered meteorological forcing. As for the absolute abundance,  
934 the enrichment of bacterial cells in the SML was also changing throughout the sampling period,  
935 with EFs ranging from 0.88 to 1.21 (Fig. 20b). A detailed investigation of physical factors (e.g.  
936 wind speed, solar radiation) driving OM concentration and bacterial abundance in the SML and  
937 bulk water will be performed to explain the short-term variability observed. During the tank  
938 experiment, cell numbers ranged between  $0.6$  and  $2.0 \times 10^6 \text{ cells mL}^{-1}$  (Fig 20c); the only  
939 exception being observed on October 3<sup>rd</sup>, when cell numbers in the SML reached  $4.9 \times 10^6 \text{ cells}$   
940  $\text{mL}^{-1}$ . Both, in the SML and bulk water, bacterial cell numbers decreased during the experiment,  
941 which may be attributed to limiting substrate supply in the closed system. Interestingly, SML  
942 cell numbers always exceeded those from the bulk water (Fig. 20d), although the SML was  
943 permanently disturbed by bursting bubbles throughout the entire experiment. This seems to be



944 in line with the high TEP concentrations observed for the SML in the tank (section 5.7.2). A  
945 recent study showed that bubbles are very effective transport vectors for bacteria into the SML,  
946 even within minutes after disruption (Robinson, et al. 2019a). The decline of SML bacterial cell  
947 numbers (both absolute and relative) during the experiment may be partly caused by permanent  
948 bacterial export into the air due to bubble bursting. Although this conclusion remains  
949 speculative as cell abundances of air samples are not available for our study, previous studies  
950 have shown that aerolisation of cells may be quite substantial (Rastelli, et al. 2017). Bacterial  
951 abundance in cloud water samples taken at the Mt. Verde during the MarParCloud campaign  
952 ranged between 0.4 and  $1.5 \times 10^5$  cells mL<sup>-1</sup> (Fig 20a). Although only few samples are available,  
953 these numbers agree well with previous reports (e.g. Hu, et al. 2018).

#### 954 5.7.4 Ice-nucleating particles

955

956 The properties of ice-nucleating particles (INP) in the SML and in bulk seawater, airborne in  
957 the marine boundary layer as well as the contribution of sea-spray aerosol particles to the INP  
958 population in clouds were examined during the campaign. The numbers of INP ( $N_{\text{INP}}$ ) at -12, -  
959 15 and -18 °C in the PM<sub>10</sub> samples from the CVAO varied from 0.000318 to 0.0232, 0.00580  
960 to 0.0533 and 0.0279 to 0.100 std L<sup>-1</sup>, respectively. INP measurements in the ocean water  
961 showed that enrichment as well as depletion of INP in SML compared to the bulk seawater  
962 occurred and enrichment factors EF varied from 0.36 to 11.40 and 0.36 to 7.11 at -15 and -20  
963 °C, respectively (details in Gong, et al. 2019b).  $N_{\text{INP}}$  (per volume of water) of the cloud water  
964 was roughly similar or slightly above that of the SML (Fig. 21), while concentrations of sea salt  
965 were clearly lower in cloud water compared to ocean water. Assuming sea salt and the INP to  
966 be similarly distributed in both, sea and cloud water (i.e., assuming that INP would not be  
967 enriched or altered during the production of sea spray),  $N_{\text{INP}}$  is at least four orders of magnitude  
968 higher than what would be expected if all airborne INP originated from sea spray. These first  
969 measurements indicate that other sources besides the ocean, such as mineral dust or other long  
970 ranged transported particles, contributed to the local INP concentration (details in Gong, et al.  
971 2019b).

972

#### 973 5.8 The SML potential to form secondary organic aerosol particles

974

975 To explore if marine air masses exhibit a significant potential to form SOA, a Gothenburg  
976 Potential Aerosol Mass Reactor (Go:PAM) was used, that relies on providing a highly oxidizing  
977 medium reproducing atmospheric oxidation on timescales ranging from a day to several days  
978 in much shorter timescales (i.e., a few minutes). During the campaign, outdoor air and gases  
979 produced from a photochemical reactor was flowed through the Go:PAM (Watne, et al. 2018),  
980 and exposed to high concentrations of OH radicals formed via the photolysis of ozone and  
981 subsequent reaction with water vapour (Zabalegui, et al. 2019 and refs. therein). The aerosol  
982 particles produced at the outlet of the OFR were monitored by means of an SMPS i.e., only size  
983 distribution and number concentration were monitored. A subset of the collected SML samples  
984 were investigated within the Go:PAM and showed varying trends briefly discussed below.



985 Ozone is known to react with iodide anions to produce different iodinated gases acting as  
986 aerosol precursors (Carpenter, et al. 2012; Carpenter and Nightingale 2015). In principle, this  
987 chemistry is mainly a bulk process and not related to the SML composition. However, a daily  
988 variation of the number of particles formed was observed (but from a very limited set of  
989 samples,  $n = 3$ ) probably related to the daily sampling conditions. To explain these observations,  
990 two different hypothesis can be postulated: (i) the ozone bulk reaction is not efficient enough  
991 for our lab-to-the-field approach, (ii) ozone is scavenged away by the organic SML constituents  
992 and the products of these reactions are producing, or not, the aerosol particles in the Go:PAM.  
993 Due to the limited number of samples, no firm conclusions can be made, but we observed the  
994 clear need to have concentrated SML samples (reproduced here by centrifugation of the  
995 authentic samples) as a prerequisite of aerosol formation which is pointing toward a specific  
996 “organic-rich” chemistry. Outdoor air masses were also investigated for their secondary mass  
997 production potential. During the campaign, northeast wind dominated i.e., predominantly clean  
998 marine air masses were collected. Those did not show any distinct diurnal difference for their  
999 secondary aerosols formation potential. However, a significant decrease of secondary organic  
1000 mass was observed on September 30<sup>th</sup>, which will be analysed in more detail.

1001

1002 5.9 The way to advanced modelling

1003

1004 5.9.1 Modelling of cloud formation and vertical transfer of ocean-derived compounds

1005

1006 Besides for the assessment of the cloud types (section 4.1.4) it is intended to apply modelling  
1007 approaches to simulate the occurrence and formation of clouds at the Mt. Verde site including  
1008 advection, wind, effective transport and vertical transport. This will allow to model chemical  
1009 multiphase processes under the given physical conditions. Furthermore, the potential vertical  
1010 transfer of ocean-derived compounds to cloud level will be modelled. To this end, the  
1011 meteorological model data by the Consortium for Small-scale Modelling-Multiscale Chemistry  
1012 Aerosol Transport Model (COSMO) (Baldauf, et al. 2011) will be used to define a vertical  
1013 meteorological data field. First simulations show that clouds frequently occurred at heights of  
1014 700 m to 800 m (Fig. 22) in strong agreement with the observations. This demonstrates that  
1015 clouds at Mt. Verde can form solely due to the local meteorological conditions and not  
1016 necessarily due to orographic effects. Accordingly, the combination of the ground-based  
1017 aerosol measurements and the in-cloud measurements at the top of Mt. Verde will be applied  
1018 to examine important chemical transformations of marine aerosol particles during horizontal  
1019 and vertical transport within the MBL. From the here presented measurements, a transfer of  
1020 ocean-derived compounds to cloud level is very likely. To link and understand both  
1021 measurement sites, in terms of important multiphase chemical pathways, more detailed  
1022 modelling studies regarding the multiphase chemistry within the marine boundary layer  
1023 combined with the impact of the horizontal and vertical transport on the aerosol and cloud  
1024 droplet composition will be performed by using different model approaches (more details in the  
1025 SI). In general, both projected model studies will focus on (i) determining the oxidation  
1026 pathways of key marine organics and (ii) the evolution of aerosol and cloud droplet acidity by



1027 chemical aging of the sea spray aerosol. The model results will finally be linked to the  
1028 measurements and compared with the measured aerosol particle concentration and composition  
1029 and the in-cloud measurements at the top of the Mt. Verde.

1030

1031 5.9.2 Development of a new organic matter emission source function

1032

1033 The link of ocean biota with marine derived organic aerosol particles has been recognized (e.g.  
1034 O'Dowd, et al. 2004). However, the usage of a single parameter like chl-*a* as indicator for  
1035 biological processes and its implementation in oceanic emission parameterisations is  
1036 insufficient as it does not reflect pelagic community structure and associated ecosystem  
1037 functions. It is strongly suggested to incorporate process-based models for marine biota and  
1038 OM rather than relying on a simple parameterizations (Burrows, et al. 2014). A major challenge  
1039 is the high level of complexity of the OM in marine aerosol particles as well as in the bulk water  
1040 and the SML as potential sources. Within MarParCloud modelling, a new source function for  
1041 the oceanic emission of OM will be developed as a combination of the sea spray source function  
1042 of Salter, et al. (2015) and a new scheme for the enrichment of OM within the emitted sea spray  
1043 droplets. This new scheme will be based on the Langmuir-Adsorption of organic species at the  
1044 bubble films. The oceanic emissions will be parameterised following Burrows, et al. (2014),  
1045 where the OM is partitioned into several classes based on their physicochemical properties. The  
1046 measured concentration of the species in the ocean surface water and the SML (e.g. lipids,  
1047 sugars and proteins) will be included in the parameterisation scheme. Finally, size class  
1048 resolved enrichment functions of the organic species groups within the jet droplets will be  
1049 implemented in the new scheme. The new emission scheme will be implemented to the aerosol  
1050 model MUSCAT (Multi-Scale Chemistry Aerosol Transport) and be validated via small and  
1051 meso-scale simulations using COSMO-MUSCAT (Wolke, et al. 2004).

1052 6 Summary and Conclusion

1053 Within MarParCloud and with substantial contributions from MARSU, an interdisciplinary  
1054 campaign in the remote tropical ocean took place in autumn 2017. This paper delivers a  
1055 description of the measurement objectives including first results and provides an overview for  
1056 upcoming detailed investigations.

1057 Typical for the measurement site, the wind direction was almost constant from the north-  
1058 easterly sector (30 – 60 °). The analysis of the air masses and dust measurements showed that  
1059 dust input was generally low, however, partly moderate dust influences were observed. Based  
1060 on very similar particle number size distributions at the ground and mountain sites, it was found  
1061 that the MBL was generally well mixed with a few exceptions and the MBL height ranged from  
1062 600 to 1100 m. Differences in the PNSDs arose from the dust influences. The chemical  
1063 composition of the aerosol particles and the cloud water indicated that the coarse mode particles  
1064 served as efficient CCN. Furthermore, lipid biomarkers were present in the aerosol particles in  
1065 typical concentrations of marine background conditions and anti-correlated with dust  
1066 concentrations.



1067 From the satellite cloud observations and supporting modelling studies, it was suggested that  
1068 the majority of low-level clouds observed over the islands formed over the ocean and could  
1069 form solely due to the local meteorological conditions. Therefore, ocean-derived aerosol  
1070 particles, e.g. sea salt and marine biogenic compounds, might be expected to have some  
1071 influence on cloud formation. The presence of compounds of marine origin in cloud water  
1072 samples (e.g. sodium, methane sulfonic acid, TEP, distinct DOM classes) at the Mt. Verde  
1073 supported an ocean-cloud link. The transfer of ocean-derived compounds, e.g. TEP, from the  
1074 ocean to the atmosphere was confirmed in controlled tank measurements. The DOM  
1075 composition of the cloud waters was consistent with the SML and bulk water composition and  
1076 partly different from the aerosol particle's composition. However, INP measurements indicated  
1077 that other sources besides the ocean and/or atmospheric transformations significantly contribute  
1078 to the local INP concentration.

1079 The bulk water and SML analysis comprised a wide spectrum of biological and chemical  
1080 constituents and consistently showed enrichment in the SML. Especially for the complex OM  
1081 characterisation, some of the methods presented here have been used for the first time for such  
1082 diverse sets of marine samples (e.g. DOM fractioning, metabolome studies with DART-HR-  
1083 MS). Chl-*a* concentrations were typical for oligotrophic regions such as Cape Verde. The  
1084 pigment composition indicated the presence of cyanobacteria, haptophytes and diatoms with a  
1085 temporal change in dominating groups (from cyanobacteria to diatoms) suggests the start of the  
1086 diatom bloom. Possible linkages to the background dust input will be resolved. Concentrations  
1087 and SML enrichment of DOC were comparable to previous campaigns at the same location. .  
1088 For the DOC as a sum parameter, the two applied sampling devices (manual and catamaran  
1089 glass plate) provided very similar results. However, if this is also true for the various compound  
1090 classes remains to be evaluated. Lipids established an important organic compound group in  
1091 the SML and a selective enrichment of surface-active lipid classes within the SML was found.  
1092 Observed enrichments also indicated on biotic and/or abiotic lipid degradation processing  
1093 within the SML. The temporal variability of bacterial abundance was studied and provided first  
1094 co-located SML and cloud water measurements for this particular oceanic province. Whether  
1095 the strong day-to-day variability of absolute cell numbers in the SML and bulk water derived  
1096 from changing water bodies and/or altered meteorological forcing needs to be further  
1097 elucidated. Regarding mercury species, results indicate that the SML is the major compartment  
1098 where (dissolved plus particulate) Hg were enriched, while MeHg was more likely concentrated  
1099 in the bulk water, underlining the importance of SML in Hg enrichment dependent on OM.

1100 For the trace gases, a variety of conditions were observed showing influences from ocean as  
1101 well as long-range transport of pollutants. High sunlight and high humidity in this tropical  
1102 region are key in ensuring that primary and secondary pollutants (e.g. ethene and ozone) are  
1103 removed effectively, however additional processes need to be regarded. Measurements within  
1104 the marine boundary layer and at the ocean-atmosphere interface, such as those shown here, are  
1105 essential to understand the various roles of these short-lived trace gases with respect to  
1106 atmospheric variability and wider climatic changes. The Cape Verde islands are likely a source  
1107 region for HONO and the potential of the SML to form secondary particles needs to be further  
1108 elucidated.

1109 This paper shows the proof of concept of the connection between organic matter emission from  
1110 the ocean to the atmosphere and up to the cloud level. We clearly see a link between the ocean



1111 and the atmosphere as (i) the particles measured at the surface are well mixed within the marine  
1112 boundary layer up to cloud level and (ii) ocean-derived compounds can be found in the aerosol  
1113 particles at mountain height and in the cloud water. The organic measurements will be  
1114 implemented in a new source function for the oceanic emission of OM. From a perspective of  
1115 particle number concentrations, the marine contributions to both CCN and INP are rather  
1116 limited. However, a clear description of any potential transfer patterns and the quantification of  
1117 additional important sources must await the complete analysis of all the samples collected. The  
1118 main current objective is to finalize all measurements and interconnect the meteorological,  
1119 physical, biological and chemical parameters also to be implemented as key variables in model  
1120 runs. Finally, we aim to achieve a comprehensive picture of the seawater and atmospheric  
1121 conditions for the period of the campaign to elucidate in particular the abundance and cycling  
1122 of organic matter between the marine environmental compartments.

1123

1124 *Data availability.* Data can be made available by the authors upon request.

1125

1126

1127

1128 *Appendix A1: List of acronyms*

1129

1130 APS – Aerodynamic particle sizer

1131 CCN – Cloud condensation nuclei

1132 CCNc – Cloud condensation nuclei counter

1133 CDOM – Chromophoric dissolved organic matter

1134 chl-*a* – Chlorophyll-*a*

1135 COSMO – Consortium for small-scale modelling-multiscale chemistry aerosol transport model

1136 CTD – Conductivity-temperature-depth sensor

1137 CVAO – Cape Verde atmospheric observatory

1138 CVFZ – Cape Verde frontal zone

1139 CVOO – Cape Verde ocean observatory

1140 DART-QTOF-MS – Direct analysis in real time quadrupole time-of-flight mass spectrometry

1141 DegLip – Lipid degradation products

1142 DL – Dissolved lipids

1143 DMS – Dimethyl sulfide

1144 DOC – Dissolved organic carbon

1145 DOM – Dissolved organic matter

1146 ECWMF – European center for medium-range weather forecasts

1147 EBUS – Eastern-boundary upwelling system

1148 EF – Enrichment factor (analyte concentration in the SML in respect to the analyte concentration in  
1149 the bulk water)

1150 ETNA – Eastern tropical north Atlantic

1151 FAA – Free amino acids

1152 Go:PAM – Gothenburg potential aerosol mass reactor

1153 HONO – Nitrous acid



- 1154 HYSPLIT – Hybrid single-particle lagrangian integrated trajectory
- 1155 INP – Ice nucleating particle(s)
- 1156 LOPAP – Long path absorption photometer
- 1157 LMWA – Low molecular weight acids
- 1158 LMWN – Low molecular weight neutrals
- 1159 MarParCat – Catamaran with glass plates for SML sampling
- 1160 MarParCloud – Marine biological production, organic aerosol Particles and marine Clouds: a process chain
- 1161
- 1162 MARSU – MARine atmospheric Science Un unravelled
- 1163 MBL – Marine boundary layer
- 1164 MeHg – Methylmercury (MeHg)
- 1165 Mt. Verde – Highest point of the São Vicente island (744 m)
- 1166 MUSCAT – Multi-scale chemistry aerosol transport
- 1167 NACW – North Atlantic central water masses
- 1168  $N_{CCN}$  – Cloud condensation nuclei number concentration
- 1169  $N_{INP}$  – Numbers of INP
- 1170 OH – Hydroxyl radical
- 1171 OFR – Oxidation flow reactor
- 1172 OM – Organic matter
- 1173 OMZ – Oxygen minimum zone
- 1174 (O)VOC – (Oxygenated) volatile organic compounds
- 1175  $PM_1$  – Particulate matter (aerosol particles) smaller than 1  $\mu m$
- 1176  $PM_{10}$  – Particulate matter (aerosol particles) smaller than 10  $\mu m$
- 1177 PNSDs – Particle number size distributions
- 1178 POM – Particulate organic matter
- 1179 PVM – Particle volume monitor
- 1180 SACW – South Atlantic central water mass
- 1181 SAL – Saharan air layer
- 1182 SAS – Surface-active substances/surfactants
- 1183 SML – Sea surface microlayer
- 1184 SOA – Secondary organic aerosol
- 1185 SSA – Sea spray aerosol
- 1186 SMPS – Scanning mobility particle sizer
- 1187 TEP – Transparent exopolymer particles
- 1188 TSP – Total suspended particle
- 1189 TM – Transmission mode
- 1190 WSOM – Water-soluble organic matter
- 1191
- 1192

#### 1193 Acknowledgement

1194 This work was funded by Leibniz Association SAW in the project “Marine biological  
1195 production, organic aerosol particles and marine clouds: a Process Chain (MarParCloud)”  
1196 (SAW-2016-TROPOS-2) and within the Research and Innovation Staff Exchange EU project  
1197 MARSU (69089). We acknowledge the CVAO site manager Luis Neves and to the  
1198 Atmospheric Measurement Facility at the National Centre for Atmospheric Science (AMF,  
1199 NCAS) for the funding of the trace gas measurements. We thank the European Regional



1200 Development fund by the European Union under contract no. 100188826. The authors  
1201 acknowledge Thomas Conrath, Tobias Spranger and Pit Strehl for their support in the fieldwork  
1202 Kerstin Lerche from the Helmholtz-Zentrum für Umweltforschung GmbH – UFZ in  
1203 Magdeburg is acknowledged for the pigment measurements. The authors thank Susanne Fuchs,  
1204 Anett Dietze, Sontje Krupka, René Rabe and Anke Rödger for providing additional data and  
1205 filter samples. Kay Weinhold, Thomas Müller und Alfred Wiedensohler are acknowledged for  
1206 their data support. We thank Johannes Lampel for providing the photograph of Figure 1. María  
1207 Eugenia Monge is a research staff member from CONICET (Consejo Nacional de  
1208 Investigaciones Científicas y Técnicas, Argentina). Jianmin Chen thanks for funding from the  
1209 Ministry of Science and Technology of China (No.2016YFC0202700), and National Natural  
1210 Science Foundation of China (No. 91843301, 91743202, 21527814). Sanja Frka and Blaženka  
1211 Gašparović acknowledge the Croatian Science Foundation for the full support under the  
1212 Croatian Science Foundation project IP-2018-01-3105. In addition, the use of SEVIRI data and  
1213 NWCSAF processing software distributed by EUMETSAT and obtained from the TROPOS  
1214 satellite archive is acknowledged. Erik H. Hoffmann thanks the Ph.D. scholarship program of  
1215 the German Federal Environmental Foundation (Deutsche Bundesstiftung Umwelt, DBU, AZ:  
1216 2016/424) for its financial support. Ryan Pereira thanks Juliane Bischoff and Sara Trojahn for  
1217 technical support. We also thank the Monaco Explorations programme as well as captain and  
1218 crew of MV YERSIN for supporting the Wave Glider deployment.

1219

1220 *Author contributions.* MvP, KWF, NT and HH organized and coordinated the MarParCloud  
1221 campaign. MvP, KWF, NT, CS, EB, XG, JV, HW, TBR, MR, CL, BG, TL, LW, JL, HC  
1222 participated in the campaign. All authors were involved in the analysis, data evaluation and  
1223 discussion of the results. MvP and HH wrote the manuscript with contributions from all co-  
1224 authors. All co-authors proofread and commented the manuscript.

1225 *Competing interest.* The authors declare that they have no conflict of interest.

1226

1227 References

1228 Abbatt, J. P. D., Leitch, W. R., Aliabadi, A. A., Bertram, A. K., Blanchet, J. P., Boivin-Rioux,  
1229 A., Bozem, H., Burkart, J., Chang, R. Y. W., Charette, J., Chaubey, J. P., Christensen, R. J.,  
1230 Cirisan, A., Collins, D. B., Croft, B., Dionne, J., Evans, G. J., Fletcher, C. G., Gali, M.,  
1231 Ghahremaninezhad, R., Girard, E., Gong, W. M., Gosselin, M., Gourdal, M., Hanna, S. J.,  
1232 Hayashida, H., Herber, A. B., Hesaraki, S., Hoor, P., Huang, L., Hussherr, R., Irish, V. E., Keita,  
1233 S. A., Kodros, J. K., Kollner, F., Kolonjari, F., Kunkel, D., Ladino, L. A., Law, K., Lévassieur,  
1234 M., Libois, Q., Liggio, J., Lizotte, M., Macdonald, K. M., Mahmood, R., Martin, R. V., Mason,  
1235 R. H., Miller, L. A., Moravek, A., Mortenson, E., Mungall, E. L., Murphy, J. G., Namazi, M.,  
1236 Norman, A. L., O'Neill, N. T., Pierce, J. R., Russell, L. M., Schneider, J., Schulz, H., Sharma,  
1237 S., Si, M., Staebler, R. M., Steiner, N. S., Thomas, J. L., von Salzen, K., Wentzell, J. J. B.,  
1238 Willis, M. D., Wentworth, G. R., Xu, J. W., and Yakobi-Hancock, J. D.: Overview paper: New  
1239 insights into aerosol and climate in the Arctic, *Atmos. Chem. Phys.*, 19, 2527-2560,  
1240 10.5194/acp-19-2527-2019, 2019.

1241 Baldauf, M., Seifert, A., Forstner, J., Majewski, D., Raschendorfer, M., and Reinhardt, T.:  
1242 Operational Convective-Scale Numerical Weather Prediction with the COSMO Model:



- 1243 Description and Sensitivities, *Monthly Weather Review*, 139, 3887-3905, 10.1175/mwr-d-10-  
1244 05013.1, 2011.
- 1245 Batrakova, N., Travnikov, O., and Rozovskaya, O.: Chemical and physical transformations of  
1246 mercury in the ocean: a review, *Ocean Science*, 10, 1047-1063, 10.5194/os-10-1047-2014,  
1247 2014.
- 1248 Bigg, E. K., and Leck, C.: The composition of fragments of bubbles bursting at the ocean  
1249 surface, *Journal of Geophysical Research-Atmospheres*, 113, 10.1029/2007jd009078, 2008.
- 1250 Blum, J. D., Popp, B. N., Drazen, J. C., Anela Choy, C., and Johnson, M. W.: Methylmercury  
1251 production below the mixed layer in the North Pacific Ocean, *Nature Geoscience*, 6, 879-884,  
1252 10.1038/ngeo1918, 2013.
- 1253 Bonsang, B., Gros, V., Peeken, I., Yassaa, N., Bluhm, K., Zoellner, E., Sarda-Estevé, R., and  
1254 Williams, J.: Isoprene emission from phytoplankton monocultures, relationship with  
1255 chlorophyll, cell volume, and carbon content., *Environmental Chemistry*, 7, 554-563, DOI:  
1256 10.1071/EN09156 2010.
- 1257 Bowman, K. L., Hammerschmidt, C. R., Lamborg, C. H., and Swarr, G.: Mercury in the North  
1258 Atlantic Ocean: The U.S. GEOTRACES zonal and meridional sections, *Deep Sea Research*  
1259 *Part II: Topical Studies in Oceanography*, 116, 251-261, 10.1016/j.dsr2.2014.07.004, 2015.
- 1260 Brandt, P., Bange, H. W., Banyte, D., Dengler, M., Didwischus, S. H., Fischer, T., Greatbatch,  
1261 R. J., Hahn, J., Kanzow, T., Karstensen, J., Krortzinger, A., Krahmann, G., Schmidtko, S.,  
1262 Stramma, L., Tanhua, T., and Visbeck, M.: On the role of circulation and mixing in the  
1263 ventilation of oxygen minimum zones with a focus on the eastern tropical North Atlantic,  
1264 *Biogeosciences*, 12, 489-512, 10.5194/bg-12-489-2015, 2015.
- 1265 Brooks, S. D., and Thornton, D. C. O.: Marine Aerosols and Clouds, in: *Annual Review of*  
1266 *Marine Science*, Vol 10, edited by: Carlson, C. A., and Giovannoni, S. J., *Annual Review of*  
1267 *Marine Science*, Annual Reviews, Palo Alto, 289-313, 2018.
- 1268 Brueggemann, M., Hayeck, N., and George, C.: Interfacial photochemistry at the ocean surface  
1269 is a global source of organic vapors and aerosols, *Nature Communications*, 9, 10.1038/s41467-  
1270 018-04528-7, 2018.
- 1271 Burrows, S. M., Hoose, C., Poschl, U., and Lawrence, M. G.: Ice nuclei in marine air: biogenic  
1272 particles or dust?, *Atmos. Chem. Phys.*, 13, 245-267, 10.5194/acp-13-245-2013, 2013.
- 1273 Burrows, S. M., Ogunro, O., Frossard, A. A., Russell, L. M., Rasch, P. J., and Elliott, S. M.: A  
1274 physically based framework for modeling the organic fractionation of sea spray aerosol from  
1275 bubble film Langmuir equilibria, *Atmos. Chem. Phys.*, 14, 13601-13629, 10.5194/acp-14-  
1276 13601-2014, 2014.
- 1277 Carpenter, L. J., Fleming, Z. L., Read, K. A., Lee, J. D., Moller, S. J., Hopkins, J. R., Purvis, R.  
1278 M., Lewis, A. C., Müller, K., Heinold, B., Herrmann, H., Fomba, K. W., van Pinxteren, D.,  
1279 Müller, C., Tegen, I., Wiedensohler, A., Müller, T., Niedermeier, N., Achterberg, E. P., Patey,  
1280 M. D., Kozlova, E. A., Heimann, M., Heard, D. E., Plane, J. M. C., Mahajan, A., Oetjen, H.,  
1281 Ingham, T., Stone, D., Whalley, L. K., Evans, M. J., Pilling, M. J., Leigh, R. J., Monks, P. S.,  
1282 Karunaharan, A., Vaughan, S., Arnold, S. R., Tschritter, J., Pöhler, D., Friess, U., Holla, R.,  
1283 Mendes, L. M., Lopez, H., Faria, B., Manning, A. J., and Wallace, D. W. R.: Seasonal



- 1284 characteristics of tropical marine boundary layer air measured at the Cape Verde Atmospheric  
1285 Observatory, *Journal of Atmospheric Chemistry*, 67, 87-140, 10.1007/s10874-011-9206-1,  
1286 2010.
- 1287 Carpenter, L. J., Archer, S. D., and Beale, R.: Ocean-atmosphere trace gas exchange, *Chemical*  
1288 *Society Reviews*, 41, 6473-6506, 10.1039/c2cs35121h, 2012.
- 1289 Carpenter, L. J., and Nightingale, P. D.: Chemistry and Release of Gases from the Surface  
1290 Ocean, *Chemical Reviews*, 115, 4015-4034, 10.1021/cr5007123, 2015.
- 1291 Ciuraru, R., Fine, L., van Pinxteren, M., D'Anna, B., Herrmann, H., and George, C.: Unravelling  
1292 New Processes at Interfaces: Photochemical Isoprene Production at the Sea Surface,  
1293 *Environmental Science & Technology*, 49, 13199-13205, 10.1021/acs.est.5b02388, 2015.
- 1294 Cochran, R. E., Ryder, O. S., Grassian, V. H., and Prather, K. A.: Sea Spray Aerosol: The  
1295 Chemical Link between the Oceans, Atmosphere, and Climate, *Accounts Chem. Res.*, 50, 599-  
1296 604, 10.1021/acs.accounts.6b00603, 2017.
- 1297 Ćosović, B., and Vojvodić, V.: Voltammetric analysis of surface active substances in natural  
1298 seawater, *Electroanalysis*, 10, 429-434, 10.1002/(sici)1521-4109(199805)10:6<429::Aid-  
1299 elan429>3.3.Co;2-z, 1998.
- 1300 Cunliffe, M., Engel, A., Frka, S., Gašparović, B., Guitart, C., Murrell, J. C., Salter, M., Stolle,  
1301 C., Upstill-Goddard, R., and Wurl, O.: Sea surface microlayers: A unified physicochemical and  
1302 biological perspective of the air-ocean interface, *Progress in Oceanography*, 109, 104-116,  
1303 10.1016/j.pocean.2012.08.004, 2013.
- 1304 Cunliffe, M., and Wurl, O.: "Guide to best practices to study the ocean's surface", *Occasional*  
1305 *Publications of the Marine Biological Association of the United Kingdom (Plymouth, UK)*, 118  
1306 pp., (<http://www.mba.ac.uk/NMBL/>). 2014.
- 1307 de Leeuw, G., Andreas, E. L., Anguelova, M. D., Fairall, C. W., Lewis, E. R., O'Dowd, C.,  
1308 Schulz, M., and Schwartz, S. E.: Production Flux of Sea Spray Aerosol, *Reviews of Geophysics*,  
1309 49, 10.1029/2010rg000349, 2011.
- 1310 Demoz, B. B., Collett, J. L., and Daube, B. C.: On the Caltech Active Strand Cloudwater  
1311 Collectors, *Atmos Res*, 41, 47-62, Doi 10.1016/0169-8095(95)00044-5, 1996.
- 1312 Derrien, M., and Le Gleau, H.: MSG/SEVIRI cloud mask and type from SAFNWC,  
1313 *International Journal of Remote Sensing*, 26, 4707-4732, 10.1080/01431160500166128, 2005.
- 1314 Engel, A., Bange, H., Cunliffe, M., Burrows, S., Friedrichs, G., Galgani, L., Herrmann, H.,  
1315 Hertkorn, N., Johnson, M., Liss, P., Quinn, P., Schartau, M., Soloviev, A., Stolle, C., Upstill-  
1316 Goddard, R., van Pinxteren, M., and Zäncker, B.: The Ocean's Vital Skin: Toward an Integrated  
1317 Understanding of the Sea Surface Microlayer, *Front. Mar. Sci.*, 4, doi:  
1318 10.3389/fmars.2017.00165, 2017.
- 1319 Facchini, M. C., Rinaldi, M., Decesari, S., Carbone, C., Finessi, E., Mircea, M., Fuzzi, S.,  
1320 Ceburnis, D., Flanagan, R., Nilsson, E. D., de Leeuw, G., Martino, M., Woeltjen, J., and  
1321 O'Dowd, C. D.: Primary submicron marine aerosol dominated by insoluble organic colloids and  
1322 aggregates, *Geophysical Research Letters*, 35, 10.1029/2008gl034210, 2008.



- 1323 Fiedler, B., Grundle, D. S., Schutte, F., Karstensen, J., Loscher, C. R., Hauss, H., Wagner, H.,  
1324 Loginova, A., Kiko, R., Silva, P., Tanhua, T., and Kortzinger, A.: Oxygen utilization and  
1325 downward carbon flux in an oxygen-depleted eddy in the eastern tropical North Atlantic,  
1326 Biogeosciences, 13, 5633-5647, 10.5194/bg-13-5633-2016, 2016.
- 1327 Fomba, K. W., Müller, K., van Pinxteren, D., and Herrmann, H.: Aerosol size-resolved trace  
1328 metal composition in remote northern tropical Atlantic marine environment: case study Cape  
1329 Verde islands, Atmos. Chem. Phys., 13, 4801-4814, 10.5194/acp-13-4801-2013, 2013.
- 1330 Fomba, K. W., Mueller, K., van Pinxteren, D., Poulain, L., van Pinxteren, M., and Herrmann,  
1331 H.: Long-term chemical characterization of tropical and marine aerosols at the Cape Verde  
1332 Atmospheric Observatory (CVAO) from 2007 to 2011, Atmos. Chem. Phys., 14, 8883-8904,  
1333 10.5194/acp-14-8883-2014, 2014.
- 1334 Franklin, D., Poulton, J. A., Steinke, M., Young, J., Peeken, I., and Malin, G.:  
1335 Dimethylsulphide, DMSP-lyase activity and microplankton community structure inside and  
1336 outside of the Mauritanian upwelling, Progress in Oceanography, 83, 134-142, 2009.
- 1337 Frka, S., Kozarac, Z., and Čosović, B.: Characterization and seasonal variations of surface  
1338 active substances in the natural sea surface micro-layers of the coastal Middle Adriatic stations,  
1339 Estuarine Coastal and Shelf Science, 85, 555-564, 10.1016/j.ecss.2009.09.023, 2009.
- 1340 Frka, S., Pogorzelski, S., Kozarac, Z., and Čosović, B.: Physicochemical Signatures of Natural  
1341 Sea Films from Middle Adriatic Stations, Journal of Physical Chemistry A, 116, 6552-6559,  
1342 10.1021/jp212430a, 2012.
- 1343 Gantt, B., and Meskhidze, N.: The physical and chemical characteristics of marine primary  
1344 organic aerosol: a review, Atmos. Chem. Phys., 13, 3979-3996, 10.5194/acp-13-3979-2013,  
1345 2013.
- 1346 Garrett, W. D.: Collection of slick-forming materials from the sea surface, Limnol. Oceanogr.,  
1347 10, 602-605, 1965.
- 1348 Gašparović, B., Kozarac, Z., Saliot, A., Čosović, B., and Möbius, D.: Physicochemical  
1349 characterization of natural and ex-situ reconstructed sea-surface microlayers, Journal of Colloid  
1350 and Interface Science, 208, 191-202, 10.1006/jcis.1998.5792, 1998a.
- 1351 Gašparović, B., Vojvodić, V., and Čosović, B.: Excretion of organic matter during an  
1352 experimental phytoplankton bloom followed using o-nitrophenol as an electrochemical probe,  
1353 Croatica Chemica Acta, 71, 271-284, 1998b.
- 1354 Gašparović, B., Plavšić, M., Čosović, B., and Saliot, A.: Organic matter characterization in the  
1355 sea surface microlayers in the subarctic Norwegian fjords region, Marine Chemistry, 105, 1-14,  
1356 10.1016/j.marchem.2006.12.010, 2007.
- 1357 Gong, X., Wex, H., van Pinxteren, M., Triesch, N., Fomba, K. W., Lubitz, J., Stolle, C.,  
1358 Robinson, T.-B., Müller, T., Herrmann, H., and Stratmann, F.: Characterization of aerosol  
1359 particles at Cape Verde close to sea and cloud level heights – Part 2: ice nucleating particles in  
1360 air, cloud and seawater, Atmos. Chem. Phys. Discuss., <https://doi.org/10.5194/acp-2019-729>,  
1361 2019b.



- 1362 Gong, X., Wex, H., Voigtländer, J., Fomba, K. W., Weinhold, K., van Pinxteren, M., Henning,  
1363 S., Müller, T., Herrmann, H., and Stratmann, F.: Characterization of aerosol particles at Cape  
1364 Verde close to sea and cloud level heights – Part 1: particle number size distribution, cloud  
1365 condensation nuclei and their origins, <https://doi.org/10.5194/acp-2019-585>, Atmos. Chem.  
1366 Phys. Discuss, <https://doi.org/10.5194/acp-2019-585>, 2019a.
- 1367 Hepach, H., Quack, B., Ziska, F., Fuhlbrügge, S., Atlas, E., Peeken, I., Krüger, K., and Wallace,  
1368 D. W. R.: Drivers of diel and regional variations of halocarbon emissions from the tropical  
1369 North East Atlantic, Atmos. Chem. Phys., 14, 1255–1275, [10.5194/acp-14-1255-2014](https://doi.org/10.5194/acp-14-1255-2014), 2014.
- 1370 Herrmann, H., Schaefer, T., Tilgner, A., Styler, S. A., Weller, C., Teich, M., and Otto, T.:  
1371 Tropospheric Aqueous-Phase Chemistry: Kinetics, Mechanisms, and Its Coupling to a  
1372 Changing Gas Phase, Chemical Reviews, 115, 4259-4334, [10.1021/cr500447k](https://doi.org/10.1021/cr500447k), 2015.
- 1373 Hoppel, W. A., Frick, G. M., and Larson, R. E.: Effect of nonprecipitating clouds on the aerosol  
1374 size distribution in the marine boundary-layer, Geophysical Research Letters, 13, 125-128,  
1375 [10.1029/GL013i002p00125](https://doi.org/10.1029/GL013i002p00125), 1986.
- 1376 Horowitz, L. W., Walters, S., Mauzerall, D. L., Emmons, L. K., Rasch, P. J., Granier, C., Tie,  
1377 X. X., Lamarque, J. F., Schultz, M. G., Tyndall, G. S., Orlando, J. J., and Brasseur, G. P.: A  
1378 global simulation of tropospheric ozone and related tracers: Description and evaluation of  
1379 MOZART, version 2, Journal of Geophysical Research-Atmospheres, 108,  
1380 [10.1029/2002jd002853](https://doi.org/10.1029/2002jd002853), 2003.
- 1381 Hu, W., Niu, H. Y., Murata, K., Wu, Z. J., Hu, M., Kojima, T., and Zhang, D. Z.: Bacteria in  
1382 atmospheric waters: Detection, characteristics and implications, Atmos. Environ., 179, 201-  
1383 221, [10.1016/j.atmosenv.2018.02.026](https://doi.org/10.1016/j.atmosenv.2018.02.026), 2018.
- 1384 Huber, S. A., Balz, A., Abert, M., and Pronk, W.: Characterisation of aquatic humic and non-  
1385 humic matter with size-exclusion chromatography–organic carbon detection–organic nitrogen  
1386 detection (LC-OCD-OND), Water research, 45, 879-885, 2011.
- 1387 Karstensen, J., Fiedler, B., Schutte, F., Brandt, P., Kortzinger, A., Fischer, G., Zantopp, R.,  
1388 Hahn, J., Visbeck, M., and Wallace, D.: Open ocean dead zones in the tropical North Atlantic  
1389 Ocean, Biogeosciences, 12, 2597-2605, [10.5194/bg-12-2597-2015](https://doi.org/10.5194/bg-12-2597-2015), 2015.
- 1390 Kawamura, K., Ishimura, Y., and Yamazaki, K.: Four years' observations of terrestrial lipid  
1391 class compounds in marine aerosols from the western North Pacific, Global Biogeochemical  
1392 Cycles, 17, 2003.  
1393
- 1394 Kaylor, A., Dwivedi, P., Pittman, J. J., Monge, M. E., Cheng, G., Li, S., and Fernandez, F. M.:  
1395 Plasma-spray ionization (PLASI): a multimodal atmospheric pressure ion source for liquid  
1396 stream analysis, Journal of the American Society for Mass Spectrometry, 25, 1788-1793,  
1397 [10.1007/s13361-014-0948-2](https://doi.org/10.1007/s13361-014-0948-2), 2014.
- 1398 Kroflič, A., Frka, S., Simmel, M., Wex, H., and Grgić, I.: Size-Resolved Surface-Active  
1399 Substances of Atmospheric Aerosol: Reconsideration of the Impact on Cloud Droplet  
1400 Formation, Environmental Science & Technology, 52, 9179-9187, [10.1021/acs.est.8b02381](https://doi.org/10.1021/acs.est.8b02381),  
1401 2018.



- 1402 Law, C. S., Breviere, E., de Leeuw, G., Garcon, V., Guieu, C., Kieber, D. J., Konradowitz, S.,  
1403 Paulmier, A., Quinn, P. K., Saltzman, E. S., Stefels, J., and von Glasow, R.: Evolving research  
1404 directions in Surface Ocean-Lower Atmosphere (SOLAS) science, *Environmental Chemistry*,  
1405 10, 1-16, 10.1071/en12159, 2013.
- 1406 Lewis, A. C., Hopkins, J. R., Carpenter, L. J., Stanton, J., Read, K. A., and Pilling, M. J.:  
1407 Sources and sinks of acetone, methanol, and acetaldehyde in North Atlantic marine air, *Atmos.*  
1408 *Chem. Phys.*, 5, 1963-1974, 10.5194/acp-5-1963-2005, 2005.
- 1409 Li, T., Wang, Y., Mao, H., Wang, S., Talbot, R. W., Zhou, Y., Wang, Z., Nie, X., and Qie, G.:  
1410 Insights on Chemistry of Mercury Species in Clouds over Northern China: Complexation and  
1411 Adsorption, *Environ Sci Technol*, 52, 5125-5134, 10.1021/acs.est.7b06669, 2018.
- 1412 Marandino, C. A., De Bruyn, W. J., Miller, S. D., and Saltzman, E. S.: DMS air/sea flux and  
1413 gas transfer coefficients from the North Atlantic summertime coccolithophore bloom,  
1414 *Geophysical Research Letters*, 35, 10.1029/2008gl036370, 2008.
- 1415 McCluskey, C. S., Hill, T. C. J., Humphries, R. S., Rauker, A. M., Moreau, S., Stratton, P. G.,  
1416 Chambers, S. D., Williams, A. G., McRobert, I., Ward, J., Keywood, M. D., Harnwell, J.,  
1417 Ponsonby, W., Loh, Z. M., Krummel, P. B., Protat, A., Kreidenweis, S. M., and DeMott, P. J.:  
1418 Observations of Ice Nucleating Particles Over Southern Ocean Waters, *Geophysical*  
1419 *Research Letters*, 45: 11989-97 2018a.  
1420
- 1421 McCluskey, C. S., Ovadnevaite, J., Rinaldi, M., Atkinson, J., Belosi, F., Ceburnis, D., Marullo,  
1422 S., Hill, T. C. J., Lohmann, U., Kanji, Z. A., O'Dowd, C., Kreidenweis, S. M., and DeMott, P.  
1423 J.: Marine and Terrestrial Organic Ice-Nucleating Particles in Pristine Marine to Continentally  
1424 Influenced Northeast Atlantic Air Masses, *Journal of Geophysical Research-Atmospheres*, 123:  
1425 6196-212, 2018b.  
1426
- 1427 McKay, W. A., Turner, M. F., Jones, B. M. R., and Halliwell, C. M.: Emissions of hydrocarbons  
1428 from marine phytoplankton - Some results from controlled laboratory experiments, *Atmos.*  
1429 *Environ.*, 30, 2583-2593, 10.1016/1352-2310(95)00433-5, 1996.
- 1430 Middlebrook, A. M., Murphy, D. M., and Thomson, D. S.: Observations of organic material in  
1431 individual marine particles at Cape Grim during the First Aerosol Characterization Experiment  
1432 (ACE 1), *Journal of Geophysical Research: Atmospheres*, 103, 16475-16483,  
1433 10.1029/97JD03719, 1998.
- 1434 Mochida, M., Kitamori, Y., Kawamura, K., Nojiri, Y., and K. Suzuki. K.: Fatty acids in the  
1435 marine atmosphere: Factors governing their concentrations and evaluation of organic films on  
1436 sea-salt particles, *Journal of Geophysical Research-Atmospheres*, 107, 2001.  
1437
- 1438 Müller, C., Iinuma, Y., Karstensen, J., van Pinxteren, D., Lehmann, S., Gnauk, T., and  
1439 Herrmann, H.: Seasonal variation of aliphatic amines in marine sub-micrometer particles at the  
1440 Cape Verde islands, *Atmos. Chem. Phys.*, 9, 9587-9597, 2009.
- 1441 Müller, K., Lehmann, S., van Pinxteren, D., Gnauk, T., Niedermeier, N., Wiedensohler, A.,  
1442 Herrmann, H.: Particle characterization at the Cape Verde atmospheric observatory during the  
1443 2007 RHaMBLe intensive, *Atmos. Chem. Phys.*, 10: 2709-21, 2010.  
1444



- 1445 Mustaffa, N. I. H., Ribas-Ribas, M., and Wurl, O.: High-resolution variability of the enrichment  
1446 of fluorescence dissolved organic matter in the sea surface microlayer of an upwelling region,  
1447 *Elementa-Science of the Anthropocene*, 5, 10.1525/elementa.242, 2017.
- 1448 Mustaffa, N. I. H., Badewien, T. H., Ribas-Ribas, M., and Wurl, O.: High-resolution  
1449 observations on enrichment processes in the sea-surface microlayer, *Scientific Reports*, 8,  
1450 10.1038/s41598-018-31465-8, 2018.
- 1451 O'Dowd, C. D., Facchini, M. C., Cavalli, F., Ceburnis, D., Mircea, M., Decesari, S., Fuzzi, S.,  
1452 Yoon, Y. J., and Putaud, J. P.: Biogenically driven organic contribution to marine aerosol,  
1453 *Nature*, 431, 676-680, Doi 10.1038/Nature02959, 2004.
- 1454 Ovadnevaite, J., O'Dowd, C., Dall'Osto, M., Ceburnis, D., Worsnop, D. R., and Berresheim,  
1455 H.: Detecting high contributions of primary organic matter to marine aerosol: A case study,  
1456 *Geophysical Research Letters*, 38, 10.1029/2010gl046083, 2011.
- 1457 Pagnone, A., Volker, C., and Ye, Y.: Processes affecting dissolved iron across the Subtropical  
1458 North Atlantic: a model study, *Ocean Dyn.*, 69, 989-1007, 10.1007/s10236-019-01288-w,  
1459 2019.
- 1460 Pastor, M. V., Pelegri, J. L., Hernandez-Guerra, A., Font, J., Salat, J., and Emellanov, M.: Water  
1461 and nutrient fluxes off Northwest Africa, *Continental Shelf Research*, 28, 915-936,  
1462 10.1016/j.csr.2008.01.011, 2008.
- 1463 Patey, M. D., Achterberg, E. P., Rijkenberg, M. J., and Pearce, R.: Aerosol time-series  
1464 measurements over the tropical Northeast Atlantic Ocean: Dust sources, elemental composition  
1465 and mineralogy, *Marine Chemistry*, 174, 103-119, 10.1016/j.marchem.2015.06.004, 2015.
- 1466 Pereira, R., Ashton, I., Sabbaghzadeh, B., Shutler, J. D., and Upstill-Goddard, R. C.: Reduced  
1467 air-sea CO<sub>2</sub> exchange in the Atlantic Ocean due to biological surfactants, *Nature Geoscience*,  
1468 11, 492-+, 10.1038/s41561-018-0136-2, 2018.
- 1469 Petters, M. D., and Kreidenweis, S. M.: A single parameter representation of hygroscopic  
1470 growth and cloud condensation nucleus activity, *Atmos. Chem. Phys.*, 7, 1961-1971,  
1471 10.5194/acp-7-1961-2007, 2007.
- 1472 Prather, K. A., Bertram, T. H., Grassian, V. H., Deane, G. B., Stokes, M. D., DeMott, P. J.,  
1473 Aluwihare, L. I., Palenik, B. P., Azam, F., Seinfeld, J. H., Moffet, R. C., Molina, M. J., Cappa,  
1474 C. D., Geiger, F. M., Roberts, G. C., Russell, L. M., Ault, A. P., Baltrusaitis, J., Collins, D. B.,  
1475 Corrigan, C. E., Cuadra-Rodriguez, L. A., Ebben, C. J., Forestieri, S. D., Guasco, T. L., Hersey,  
1476 S. P., Kim, M. J., Lambert, W. F., Modini, R. L., Mui, W., Pedler, B. E., Ruppel, M. J., Ryder,  
1477 O. S., Schoepp, N. G., Sullivan, R. C., and Zhao, D.: Bringing the ocean into the laboratory to  
1478 probe the chemical complexity of sea spray aerosol, *Proceedings of the National Academy of  
1479 Sciences of the United States of America*, 110, 7550-7555, 10.1073/pnas.1300262110, 2013.
- 1480 Putaud, J. P., Van Dingenen, R., Mangoni, M., Virkkula, A., Raes, F., Maring, H., Prospero, J.  
1481 M., Swietlicki, E., Berg, O. H., Hillamo, R., and Mäkelä, T.: Chemical mass closure and  
1482 assessment of the origin of the submicron aerosol in the marine boundary layer and the free  
1483 troposphere at Tenerife during ACE-2, *Tellus B*, 52, 141-168, 10.1034/j.1600-  
1484 0889.2000.00056.x, 2000.



- 1485 Quinn, P. K., Collins, D. B., Grassian, V. H., Prather, K. A., and Bates, T. S.: Chemistry and  
1486 Related Properties of Freshly Emitted Sea Spray Aerosol, *Chemical Reviews*, 115, 4383-4399,  
1487 10.1021/cr500713g, 2015.
- 1488 Rahlff, J., Stolle, C., Giebel, H. A., Brinkhoff, T., Ribas-Ribas, M., Hodapp, D., and Wurl, O.:  
1489 High wind speeds prevent formation of a distinct bacterioneuston community in the sea-surface  
1490 microlayer, *Fems Microbiology Ecology*, 93, 10.1093/femsec/fix041, 2017.
- 1491 Rastelli, E., Corinaldesi, C., Dell'Anno, A., Lo Martire, M., Greco, S., Facchini, M. C., Rinaldi,  
1492 M., O'Dowd, C., Ceburnis, D., and Danovaro, R.: Transfer of labile organic matter and microbes  
1493 from the ocean surface to the marine aerosol: an experimental approach, *Scientific Reports*, 7,  
1494 10.1038/s41598-017-10563-z, 2017.
- 1495 Read, K. A., Mahajan, A. S., Carpenter, L. J., Evans, M. J., Faria, B. V. E., Heard, D. E.,  
1496 Hopkins, J. R., Lee, J. D., Moller, S. J., Lewis, A. C., Mendes, L., McQuaid, J. B., Oetjen, H.,  
1497 Saiz-Lopez, A., Pilling, M. J., and Plane, J. M. C.: Extensive halogen-mediated ozone  
1498 destruction over the tropical Atlantic Ocean, *Nature*, 453, 1232-1235, 10.1038/nature07035,  
1499 2008.
- 1500 Read, K. A., Carpenter, L. J., Arnold, S. R., Beale, R., Nightingale, P. D., Hopkins, J. R., Lewis,  
1501 A. C., Lee, J. D., Mendes, L., and Pickering, S. J.: Multiannual Observations of Acetone,  
1502 Methanol, and Acetaldehyde in Remote Tropical Atlantic Air: Implications for Atmospheric  
1503 OVOC Budgets and Oxidative Capacity, *Environmental Science & Technology*, 46, 11028-  
1504 11039, 10.1021/es302082p, 2012.
- 1505 Roberts, G. C., and Nenes, A.: A continuous-flow streamwise thermal-gradient CCN chamber  
1506 for atmospheric measurements, *Aerosol Science and Technology*, 39, 206-221,  
1507 10.1080/027868290913988, 2005.
- 1508 Robinson, T.-B., Stolle, C., and Wurl, O.: Depth is Relative: The Importance of Depth on TEP  
1509 in the Near Surface Environment, *Ocean Sci. Discuss.*, 2019a.
- 1510 Robinson, T.-B., Wurl, O., Bahlmann, E., Jürgens, K., and Stolle, C.: 2019 b. 'Rising bubbles  
1511 enhance the gelatinous nature of the air-sea interface', *Limnology and Oceanography*,  
1512 10.1002/lno.11188, 2019b.
- 1513
- 1514 Salter, M. E., Zieger, P., Navarro, J. C. A., Grythe, H., Kirkevåg, A., Rosati, B., Riipinen, I.,  
1515 and Nilsson, E. D.: An empirically derived inorganic sea spray source function incorporating  
1516 sea surface temperature, *Atmos. Chem. Phys.*, 15, 11047-11066, 10.5194/acp-15-11047-2015,  
1517 2015.
- 1518 Schepanski, K., Tegen, I., and Macke, A.: Saharan dust transport and deposition towards the  
1519 tropical northern Atlantic, *Atmos. Chem. Phys.*, 9, 1173-1189, DOI 10.5194/acp-9-1173-2009,  
1520 2009.
- 1521 Schmetz, J., Pili, P., Tjemkes, S., Just, D., Kerkmann, J., Rota, S., and Ratier, A.: An  
1522 introduction to Meteosat Second Generation (MSG), *Bulletin of the American Meteorological*  
1523 *Society*, 83, 977-+, 10.1175/BAMS-83-7-Schmetz-1, 2002.
- 1524 Simoneit, B. R. T., Chester, R., and Eglinton, G.: Biogenic lipids in particulates from lower  
1525 atmosphere over eastern Atlantic, *Nature*, 267: 682-85, 1977.
- 1526



- 1527 Simoneit, B. R. T., Kobayashi, M., Mochida, M., Kawamura, K., Lee, M., Lim, H. J., Turpin,  
1528 B. J., and Komazaki, Y.: Composition and major sources of organic compounds of aerosol  
1529 particulate matter sampled during the ACE-Asia campaign, *Journal of Geophysical Research-*  
1530 *Atmospheres*, 109, 2004.  
1531
- 1532 Stolle, C., Nagel, K., Labrenz, M., and Jürgens, K.: Succession of the sea-surface microlayer in  
1533 the coastal Baltic Sea under natural and experimentally induced low-wind conditions,  
1534 *Biogeosciences*, 7, 2975-2988, 2010.
- 1535 Stolle, C., Ribas-Ribas, M., Badewien, T.H., Barnes, J., Carpenter, L.J., Chance, R., Damgaard,  
1536 L.R., Durán Quesada, A.M., Engel, A., Frka, S., Galgani, L., Gašparović, B., Gerriets, M.,  
1537 Hamizah Mustaffa, N.I., Herrmann, H., Kallajoki, L., Pereira, R., Radach, F., Revsbech, N.P.,  
1538 Rickard, P., Saint, A., Salter, M., Striebel, M., Triesch, N., Uher, G., Upstill-Goddard, R.C., van  
1539 Pinxteren, M., Zäncker, B., Zieger, P., and Wurl, O.: The MILAN campaign: Studying diel  
1540 light effects on the air-sea interface, accepted for *Bulletin of the American Meteorological*  
1541 *Society*, 2019.  
1542
- 1543 Stramma, L., Huttel, S., and Schafstall, J.: Water masses and currents in the upper tropical  
1544 northeast Atlantic off northwest Africa, *J. Geophys. Res.-Oceans*, 110, 10.1029/2005jc002939,  
1545 2005.
- 1546 Tang, K., Page, J. S., and Smith, R. D.: Charge competition and the linear dynamic range of  
1547 detection in electrospray ionization mass spectrometry, *Journal of the American Society for*  
1548 *Mass Spectrometry*, 15, 1416-1423, 10.1016/j.jasms.2004.04.034, 2004.
- 1549 Triesch, N, van Pinxteren, M., Engel, A., and Herrmann, H.: Concerted measurements of free  
1550 amino acids at the Cape Verde Islands: High enrichments in submicron sea spray aerosol  
1551 particles and cloud droplets, submitted to *Atmos. Chem. Phys.*, 2019.  
1552
- 1553 van Pinxteren, D., Brüeggemann, E., Gnauk, T., Mueller, K., Thiel, C., and Herrmann, H.: A  
1554 GIS based approach to back trajectory analysis for the source apportionment of aerosol  
1555 constituents and its first application, *Journal of Atmospheric Chemistry*, 67, 1-28,  
1556 10.1007/s10874-011-9199-9, 2010.
- 1557 van Pinxteren, M., and Herrmann, H.: Glyoxal and methylglyoxal in Atlantic seawater and  
1558 marine aerosol particles: method development and first application during the Polarstern cruise  
1559 ANT XXVII/4, *Atmos. Chem. Phys.*, 13, 11791-11802, 10.5194/acp-13-11791-2013, 2013.
- 1560 van Pinxteren, M., Fiedler, B., van Pinxteren, D., Iinuma, Y., Koertzinger, A., and Herrmann,  
1561 H.: Chemical characterization of sub-micrometer aerosol particles in the tropical Atlantic  
1562 Ocean: marine and biomass burning influences, *Journal of Atmospheric Chemistry*, 72: 105-  
1563 25, 2015.  
1564
- 1565 van Pinxteren, M., Barthel, S., Fomba, K., Müller, K., von Tümpling, W., and Herrmann, H.:  
1566 The influence of environmental drivers on the enrichment of organic carbon in the sea surface  
1567 microlayer and in submicron aerosol particles – measurements from the Atlantic Ocean, *Elem*  
1568 *Sci Anth*, 5, <https://doi.org/10.1525/elementa.225>, 2017.



- 1569 Vaughan, S., Ingham, T., Whalley, L. K., Stone, D., Evans, M. J., Read, K. A., Lee, J. D.,  
1570 Moller, S. J., Carpenter, L. J., Lewis, A. C., Fleming, Z. L., and Heard, D. E.: Seasonal  
1571 observations of OH and HO<sub>2</sub> in the remote tropical marine boundary layer, *Atmos. Chem.*  
1572 *Phys.*, 12, 2149-2172, 10.5194/acp-12-2149-2012, 2012.
- 1573 Watne, Å. K., Psichoudaki, M., Ljungström, E., Le Breton, M., Hallquist, M., Jerksjö, M.,  
1574 Fallgren, H., Jutterström, S., and Hallquist, Å. M.: Fresh and Oxidized Emissions from In-Use  
1575 Transit Buses Running on Diesel, Biodiesel, and CNG, *Environmental Science & Technology*,  
1576 52, 7720-7728, 10.1021/acs.est.8b01394, 2018.
- 1577 Wiedensohler, A., Birmili, W., Nowak, A., Sonntag, A., Weinhold, K., Merkel, M., Wehner,  
1578 B., Tuch, T., Pfeifer, S., Fiebig, M., Fjaraa, A. M., Asmi, E., Sellegri, K., Depuy, R., Venzac,  
1579 H., Villani, P., Laj, P., Aalto, P., Ogren, J. A., Swietlicki, E., Williams, P., Roldin, P., Quincey,  
1580 P., Hüglin, C., Fierz-Schmidhauser, R., Gysel, M., Weingartner, E., Riccobono, F., Santos, S.,  
1581 Gruning, C., Faloon, K., Beddows, D., Harrison, R. M., Monahan, C., Jennings, S. G., O'Dowd,  
1582 C. D., Marinoni, A., Horn, H. G., Keck, L., Jiang, J., Scheckman, J., McMurry, P. H., Deng, Z.,  
1583 Zhao, C. S., Moerman, M., Henzing, B., de Leeuw, G., Loschau, G., and Bastian, S.: Mobility  
1584 particle size spectrometers: harmonization of technical standards and data structure to facilitate  
1585 high quality long-term observations of atmospheric particle number size distributions,  
1586 *Atmospheric Measurement Techniques*, 5, 657-685, 10.5194/amt-5-657-2012, 2012.
- 1587 Wolke, R., Knöth, O., Hellmuth, O., Schröder, W., and Renner, E.: The parallel model system  
1588 LM-MUSCAT for chemistry-transport simulations: Coupling scheme, parallelization and  
1589 application, in: *Parallel Computing: Software Technology, Algorithms, Architectures, and*  
1590 *Applications*, edited by: G.R. Joubert, W. E. N., F.J. Peters, and W.V. Walter, Elsevier,  
1591 Amsterdam, Niederlande, 363-370, 2004.
- 1592 Wurl, O., Miller, L., Ruttgers, R., and Vagle, S.: The distribution and fate of surface-active  
1593 substances in the sea-surface microlayer and water column, *Marine Chemistry*, 115, 1-9,  
1594 10.1016/j.marchem.2009.04.007, 2009.
- 1595 Wurl, O., Wurl, E., Miller, L., Johnson, K., and Vagle, S.: Formation and global distribution of  
1596 sea-surface microlayers, *Biogeosciences*, 8, 121-135, 10.5194/bg-8-121-2011, 2011.
- 1597 Wurl, O., Stolle, C., Van Thuoc, C., The Thu, P., and Mari, X.: Biofilm-like properties of the  
1598 sea surface and predicted effects on air-sea CO<sub>2</sub> exchange, *Progress in Oceanography*, 144,  
1599 15-24, 10.1016/j.pocean.2016.03.002, 2016.
- 1600 Wurl, O., Ekau, W., Landing, W. M., and Zappa, C. J.: Sea surface microlayer in a changing  
1601 ocean - A perspective, *Elementa-Science of the Anthropocene*, 5, 10.1525/elementa.228, 2017.
- 1602 Zabalegui, N., Manzi, M., Depoorter, A., Hayeck, N., Roveretto, M., Li, C., van Pinxteren, M.,  
1603 Herrmann, H., George, C., and Monge, M.E.: Seawater Analysis by Ambient Mass  
1604 Spectrometry-Based Seaomics and Implications on Secondary Organic Aerosol Formation,  
1605 submitted to *Atmos. Chem. Phys.*, 2019.
- 1606  
1607 Zäncker, B., Cunliffe, M., and Engel, A.: Bacterial Community Composition in the Sea Surface  
1608 Microlayer Off the Peruvian Coast. *Front. Microbiol.*, 9:2699. doi: 10.3389/fmicb.2018.02699,  
1609 2018.
- 1610



1611 Zindler, C., Peeken, I., Marandino, C. A., and Bange, H. W.: Environmental control on the  
1612 variability of DMS and DMSP in the Mauritanian upwelling region, *Biogeosciences*, 9, 1041-  
1613 1051, 10.5194/bg-9-1041-2012, 2012.

1614

### 1615 **Caption of Figures:**

1616 Figure 1: Illustration of the different sampling sites during the campaign.

1617 Figure 2: The residence time of the air masses calculated from 96 h (4 days) back trajectories  
1618 in ensemble mode.

1619 Figure 3: Time-series of air temperature, wind direction, wind speed, ethene, dimethyl sulfide,  
1620 methanol, acetone, ethane and ozone.

1621 Fig. 4: The measured temperature and humidity profiles at the CVAO on September 17<sup>th</sup>  
1622 using a 16 m<sup>3</sup> Helikite. From the measurements the boundary layer height was determined  
1623 (here: ~ 850 m).

1624 Fig. 5: Time series and vertical profiles of the MBL height simulated with COSMO-  
1625 MUSCAT on the N2 domain and measured with the helikite.

1626 Fig. 6: (a) ECMWF wind forecasts and (b – f) cloud scenery derived from Meteosat SEVIRI  
1627 observations for the Cape Verde Islands region using a , a state-of-the-art cloud classification  
1628 algorithm (the cloud retrieval software of the Satellite Application Facility on support to  
1629 Nowcasting and Very Short-Range Forecasting version 2016 (a) Average horizontal winds  
1630 have been derived from a 2.5 x 2.5 degree (250 km x 250 km) domain centered on Cape  
1631 Verde Islands and are plotted for each pressure level from 1000 to 250 hPa against time using  
1632 arrows. The arrow colours refer to the pressure level. Gray vertical lines mark the times of the  
1633 subsequently shown cloud scenes. (b – f) Different cloud scenes observed with Meteosat  
1634 SEVIRI for a domain of size 1500 km x 1000 km centered on the Cape Verde Islands. The  
1635 shadings refer to different cloud types derived with the cloud classification algorithm of the  
1636 NWC-SAF v2016.

1637 Fig. 7: (a) The mission track of a SV2 Wave Glider as color-coded fluorescence data derived  
1638 from a Wetlabs FLNTURT sensor installed on the vehicle (data in arbitrary units) (b).  
1639 Chlorophyll-a surface ocean concentrations derived from the MODIS-Terra satellite (mean  
1640 concentration for October 2017). Please note that logarithmic values are shown.

1641 Fig. 8: (a) The median of PNSDs of marine type (blue) and dust type2 (black), with a linear  
1642 and (b) a logarithmic scaling on the y axis, measured from September 21<sup>st</sup> 03:30:00 to  
1643 September 21<sup>st</sup> 20:00:00 (UTC) and from September 28<sup>th</sup> 09:30:00 to September 30<sup>th</sup>  
1644 18:30:00 (UTC). The error bar indicates the range between 25% and 75% percentiles.

1645 Fig. 9: (a) The median of PNSDs for marine type particle during cloud events and non-cloud  
1646 events at CVAO and MV; (b) Scatter plots of  $N_{CCN}$  at CVAO against those at MV at  
1647 supersaturation of ~ 0.30%. Slope and  $R^2$  are given.

1648 Fig.10: (a) Percentage aerosol composition at the CVAO (mean value of 5 blocks) and (b) at  
1649 the Mt. Verde (mean value of 6 blocks) between October 2<sup>nd</sup> and October 9<sup>th</sup>. Aerosol particles  
1650 were samples in five different size stages from 0.05-0.14  $\mu\text{m}$  (stage 1), 0.14-0.42  $\mu\text{m}$  (stage 2),  
1651 0.42-1.2 $\mu\text{m}$  (stage 3), 1.2-3.5  $\mu\text{m}$  (stage 4) and 3.5-10  $\mu\text{m}$  (stage 5).

1652



1653 Fig. 11: Cloud water composition for one connected sampling event between October 5<sup>th</sup> 7:45  
1654 (start, local time, UTC-1) and October 6<sup>th</sup>, 08:45 (start, local time, UTC-1).

1655 Fig. 12: Straight chain unsaturated fatty acids ( $\Sigma(c12$  to  $c33)$ ) concentrations on the  $PM_{10}$   
1656 aerosol particles versus atmospheric dust concentrations.

1657 Fig. 13: Temporal evolution of DOC concentrations in the bulk water samples along the  
1658 campaign together with the main pigment concentrations (chl-*a*, zeaxanthin and fucoxanthin)  
1659 concentrations and total cell numbers measured in the bulk water and dust concentrations in  
1660 the atmosphere (yellow background area).

1661 Fig. 14: (a) Concentrations of DOC in the SML and (b) and in the bulk watersampled for  
1662 paired glass plate (GP) and the MarParCat (cat) sampling events.

1663 Fig 15: Average enrichments (EF) of surfactants (SAS) and dissolved lipid classes indicating  
1664 organic matter degradation (DegLip).  
1665

1666 Fig. 16: Concentrations of Hg, MeHg, DOC and POC in the sea surface microlayer (SML)  
1667 and bulk water sampled on September 26<sup>th</sup> and 27<sup>th</sup> 2017.

1668 Fig. 17: DOM classes measured in all compartments. The data represent mean values of three  
1669 SML samples and the respective bulk water, three aerosol particle samples ( $PM_{10}$ ) from the  
1670 CVAO and two aerosol samples ( $PM_{10}$ ) from the Mt. Verde and four cloud water samples, all  
1671 collected between 26. – 27.09., 01. – 02.10., and 08. – 09.10.2017.

1672 Fig. 18: (a) Total TEP abundance in the SML and the bulk water as well as enrichment factor  
1673 (SML/ULW) of TEP for field samples taken in nearshore water Cape Verde; (b) together with  
1674 tank experiment with > 3 h bubbling of water collected from nearshore Cape Verde.

1675 Fig. 19: Microscopy image of TEP in TSP aerosol particles sampled at the CVAO sampled  
1676 between September 29<sup>th</sup> and 30<sup>th</sup> with a flow rate of 8 L min<sup>-1</sup>.

1677 Fig. 20: Bacterial abundance of SML and ULW from (a) field and (c) tank water samples as  
1678 well as from cloud water samples (diamonds, a) taken during the campaign are shown.  
1679 Additionally, enrichment factors (i.e. SML versus ULW) are presented (b, d). In panel a,  
1680 please note the different power values between SML/ ULW ( $10^6$  cells mL<sup>-1</sup>) and cloud water  
1681 samples ( $10^4$  cells mL<sup>-1</sup>).

1682 Fig. 21:  $N_{INP}$  of SML seawater ( $n = 9$ ) and cloud water ( $n = 13$ ) as a function of temperature.

1683 Fig. 22: Modelled 2D vertical wind field on October 5<sup>th</sup> after 12 hours of simulation time. The  
1684 model domain spans 222 km length and 1.5 km height. The black contour lines represent the  
1685 simulated cloud liquid water content (with a minimum of 0.01 g m<sup>-3</sup> and a maximum of 0.5 g  
1686 m<sup>-3</sup>). The more dense the lines, the higher the simulated liquid water content of the clouds.

1687

1688

1689

1690

1691



1692

1693

1694 Table 1. Classification of the air masses according to dust concentrations from the impactor  
1695 samples after the calculation of dust concentrations according to Fomba, et al. 2014 samples  
1696 and under considerations of backward trajectories (Fig. 2).

Start local time (UTC-1)	Stop local time (UTC-1)	Dust Conc. [ $\mu\text{g}/\text{m}^3$ ]	Classification
2017.09.18 18:18:00	2017.09.19 14:57:00	53,5	Moderate-dust
2017.09.19 16:30:00	2017.09.20 15:30:00	38,2	Moderate-dust
2017.09.20 18:00:00	2017.09.21 14:00:00	30,0	Moderate-dust
2017.09.21 15:00:00	2017.09.22 15:00:00	14,5	Low-dust
2017.09.22 16:15:00	2017.09.24 16:46:00	4,1	Marine
2017.09.24 17:30:00	2017.09.25 14:30:00	2,2	Marine
2017.09.25 16:00:00	2017.09.26 15:00:00	11,6	Low-dust
2017.09.26 15:51:33	2017.09.27 14:45:00	37,6	Moderate-dust
2017.09.27 15:30:00	2017.09.28 16:30:00	20,6	Moderate-dust
2017.09.28 18:10:00	2017.09.30 15:45:00	27,3	Moderate-dust
2017.09.30 17:05:00	2017.10.01 14:15:00	42,7	Moderate-dust
2017.10.01 15:00:00	2017.10.02 14:30:00	35,5	Moderate-dust
2017.10.02 15:42:00	2017.10.03 14:53:00	29,1	Moderate-dust
2017.10.03 15:45:00	2017.10.04 14:30:00	14,8	Low-dust
2017.10.04 15:27:00	2017.10.05 15:18:00	13,2	Low-dust
2017.10.05 16:10:00	2017.10.06 14:54:00	17,2	Low-dust
2017.10.06 16:00:00	2017.10.07 15:30:00	17,0	Low-dust
2017.10.07 16:10:00	2017.10.09 17:27:20	16,8	Low-dust
2017.10.09 18:13:00	2017.10.10 15:00:00	27,6	Moderate-dust

1697

1698

1699

1700

1701

1702

1703

1704

1705

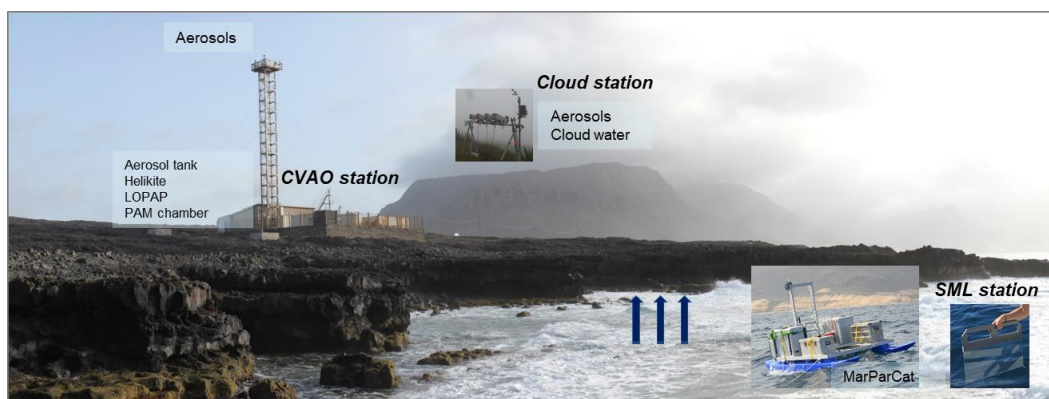
1706

1707

1708



1709



1710

1711

1712

1713

1714

1715

1716

1717

1718

1719

1720

1721

1722

1723

1724

1725

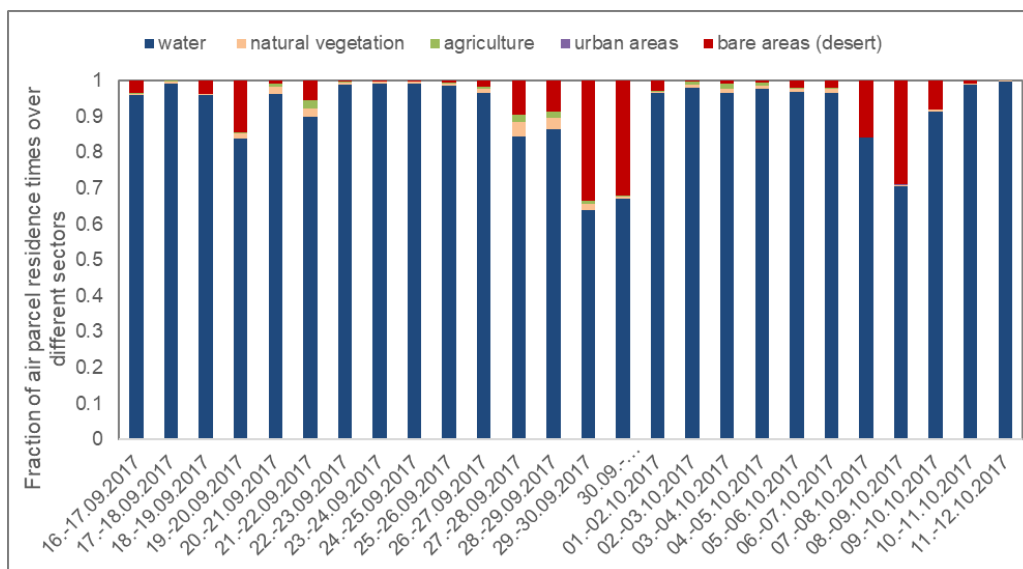
1726

1727

1728

1729

Figure 1



1730

1731

1732

1733

1734

1735

1736

1737

1738

1739

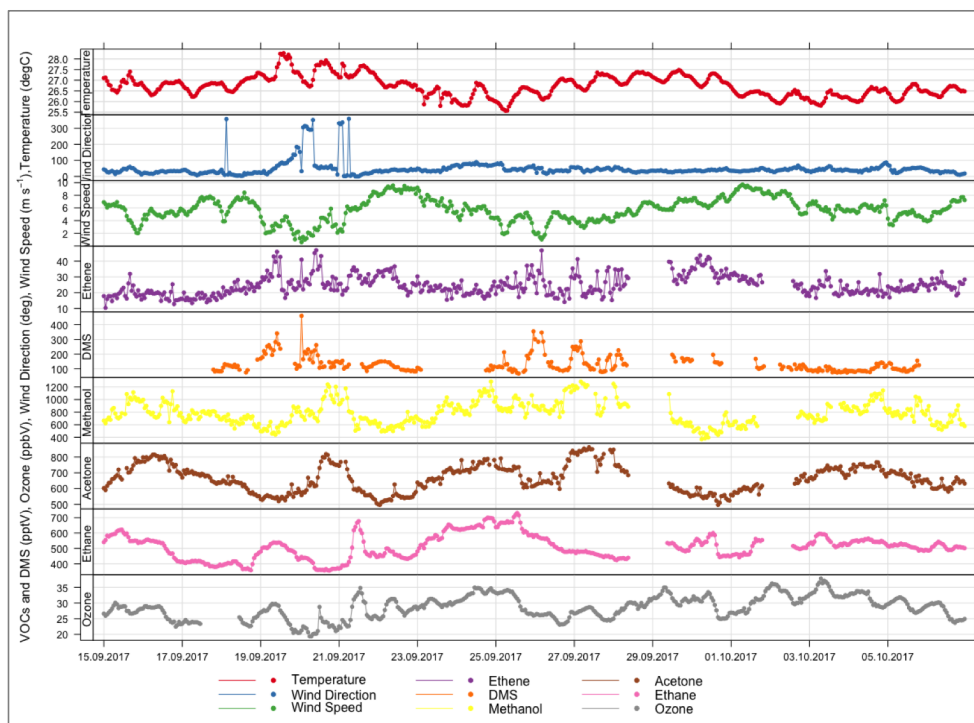
1740

1741

1742

1743

Figure 2

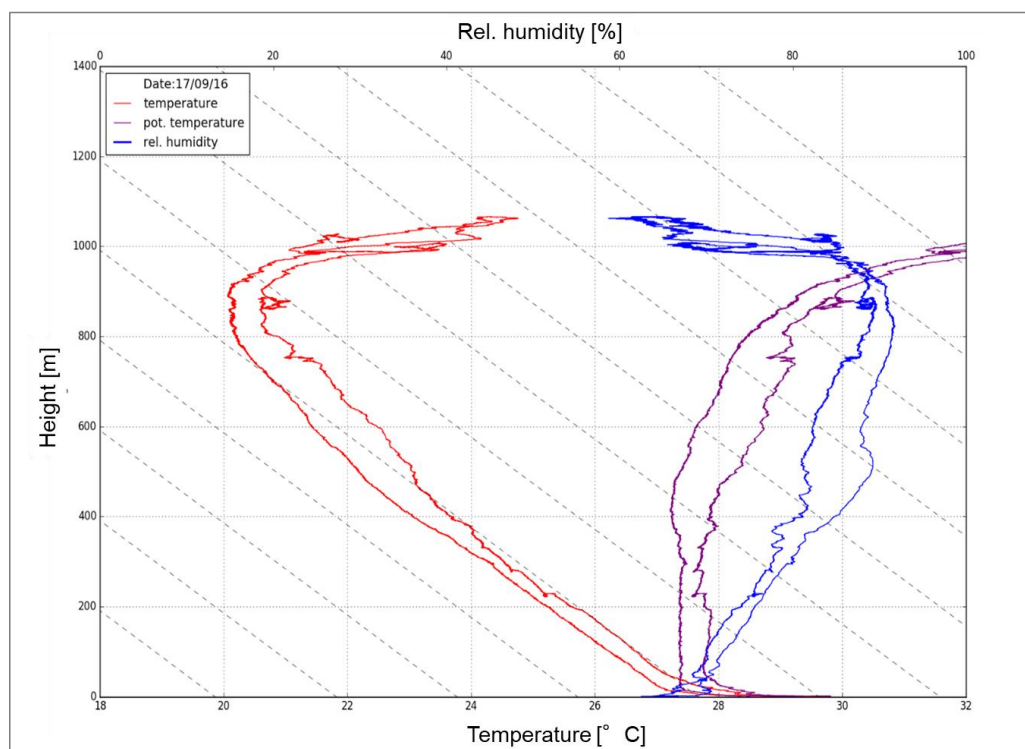


1744  
1745  
1746  
1747  
1748  
1749  
1750  
1751  
1752  
1753  
1754  
1755  
1756  
1757  
1758

Figure 3



1759



1760

1761

1762

1763

1764

1765

1766

1767

1768

1769

1770

1771

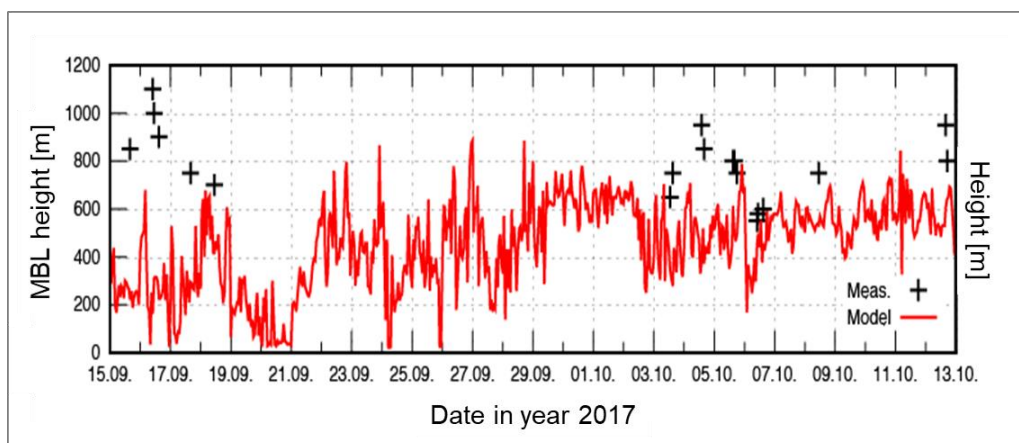
1772

1773

Figure 4



1774



1775

1776

Figure 5

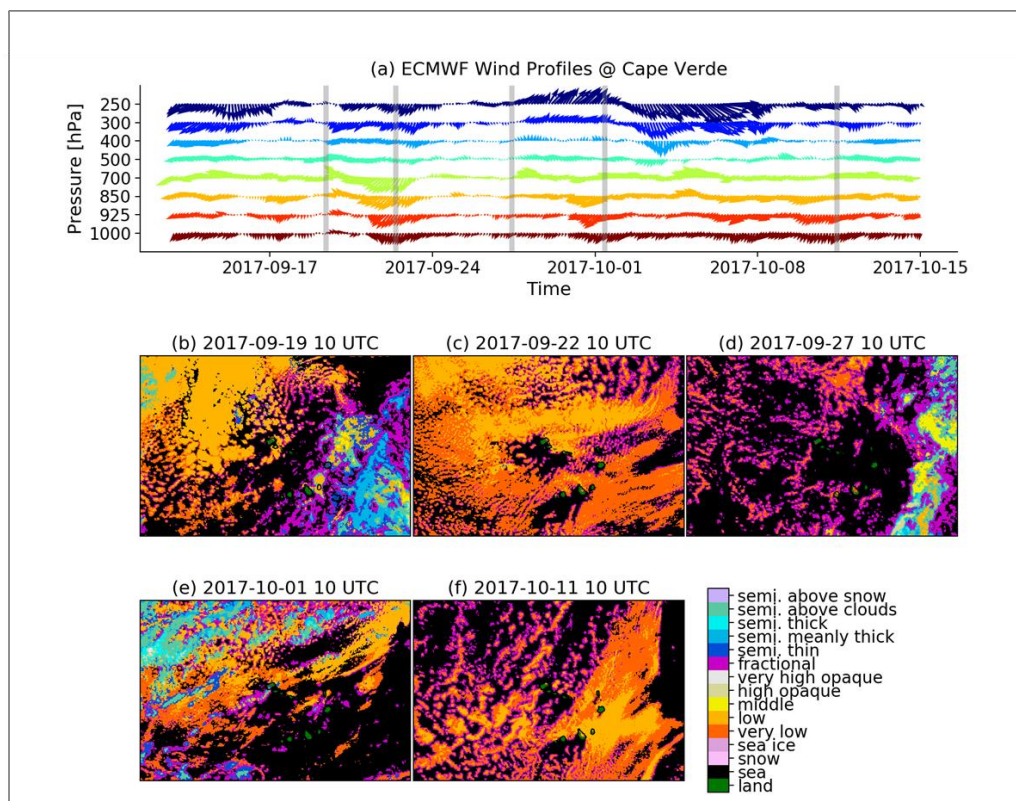
1777

1778

1779

1780

1781



1782  
1783  
1784  
1785  
1786  
1787  
1788  
1789  
1790  
1791  
1792  
1793  
1794

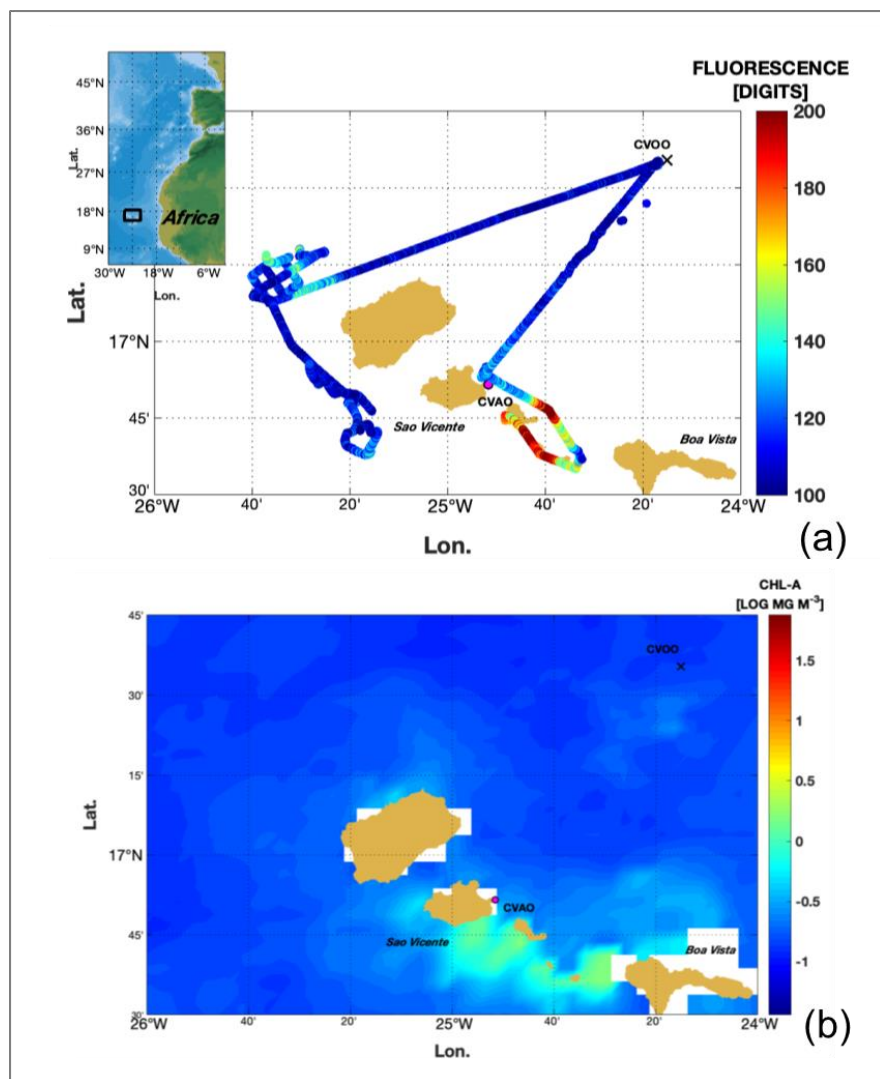
Figure 6



1795

1796

1797



1798

1799

1800

1801

1802

1803

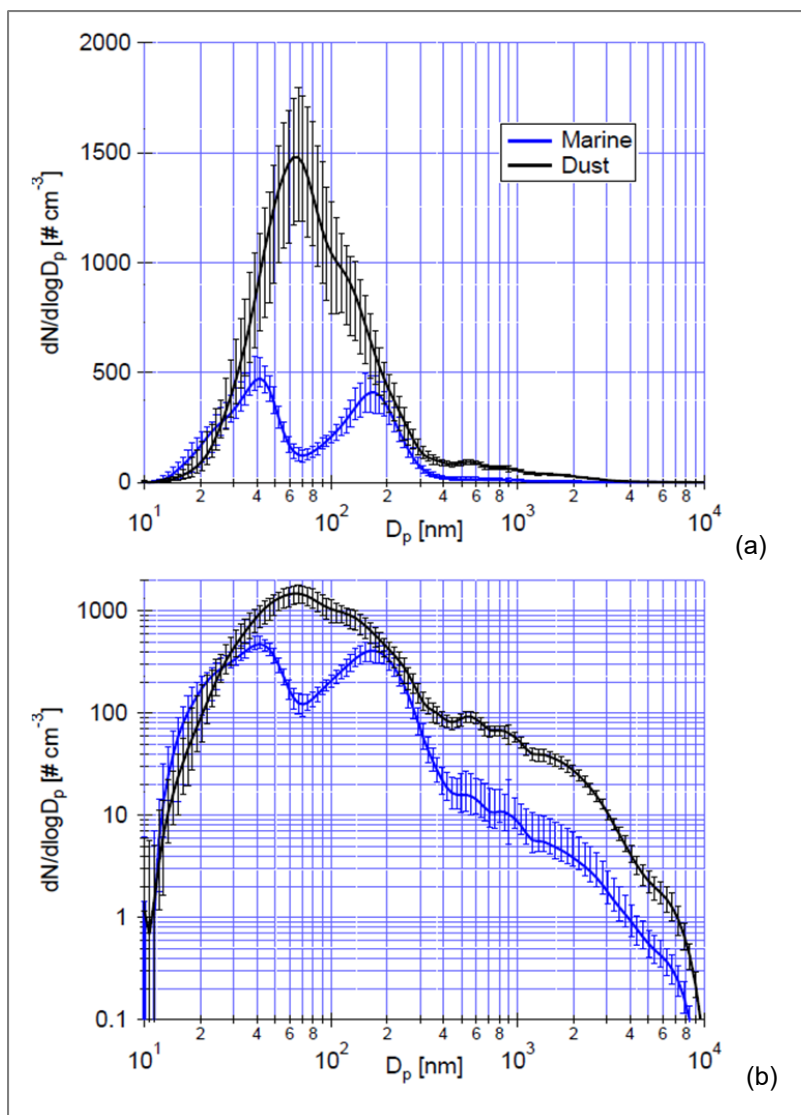
Figure 7



1804

1805

1806



1807

1808

1809

1810

1811

Figure 8



1812

1813

1814

1815

1816

1817

1818

1819

1820

1821

1822

1823

1824

1825

1826

1827

1828

1829

1830

1831

1832

1833

1834

1835

1836

1837

1838

1839

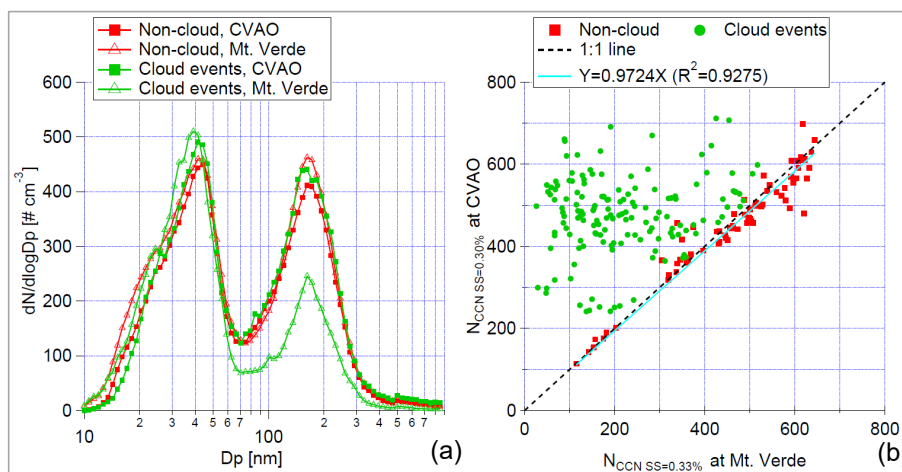


Figure 9

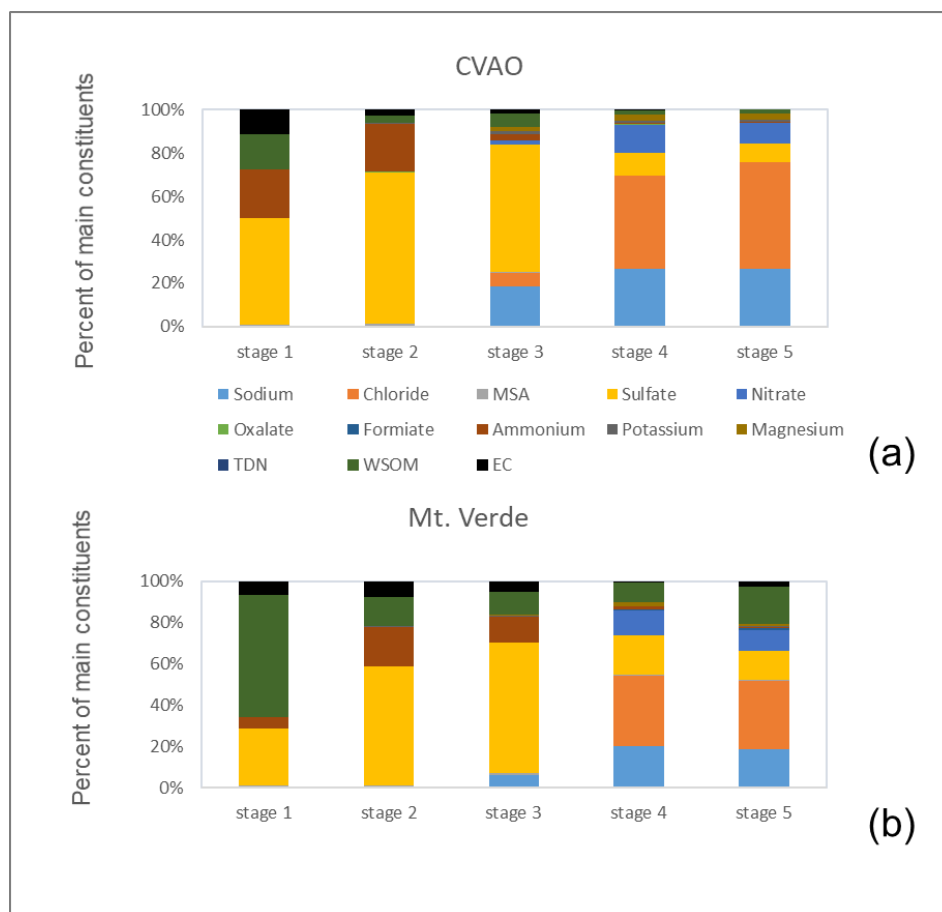


1840

1841

1842

1843



1844

1845

1846

1847

1848

1849

1850

1851

Figure 10



1852

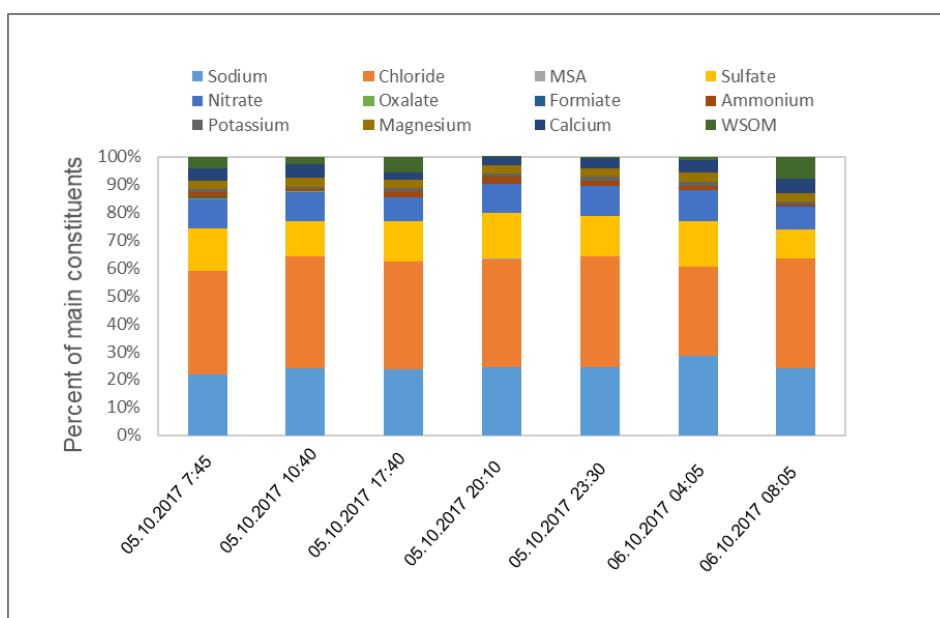
1853

1854

1855

1856

1857



1858

1859

1860

1861

1862

1863

1864

1865

1866

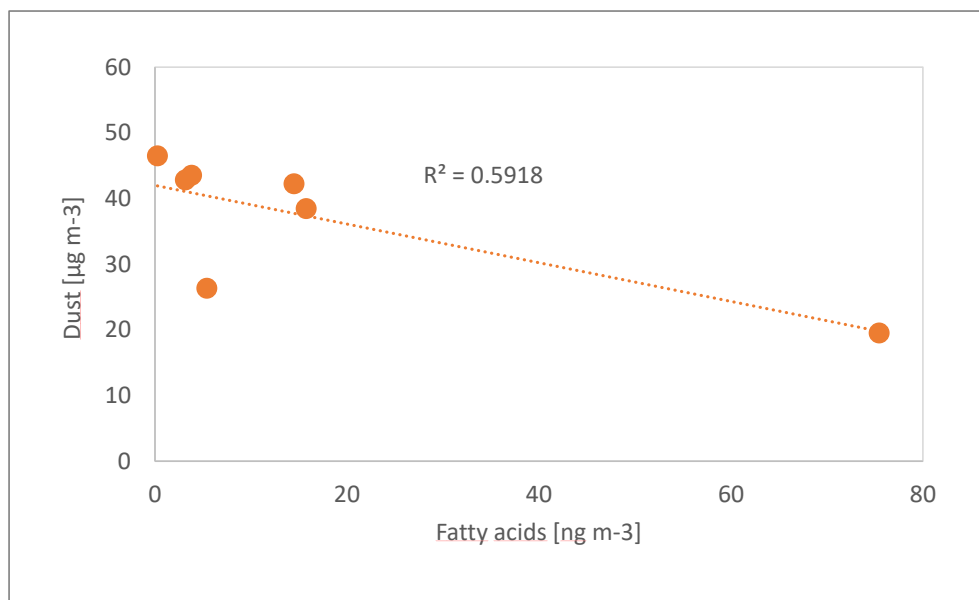
1867

1868

Figure 11



1869  
1870  
1871  
1872  
1873  
1874  
1875

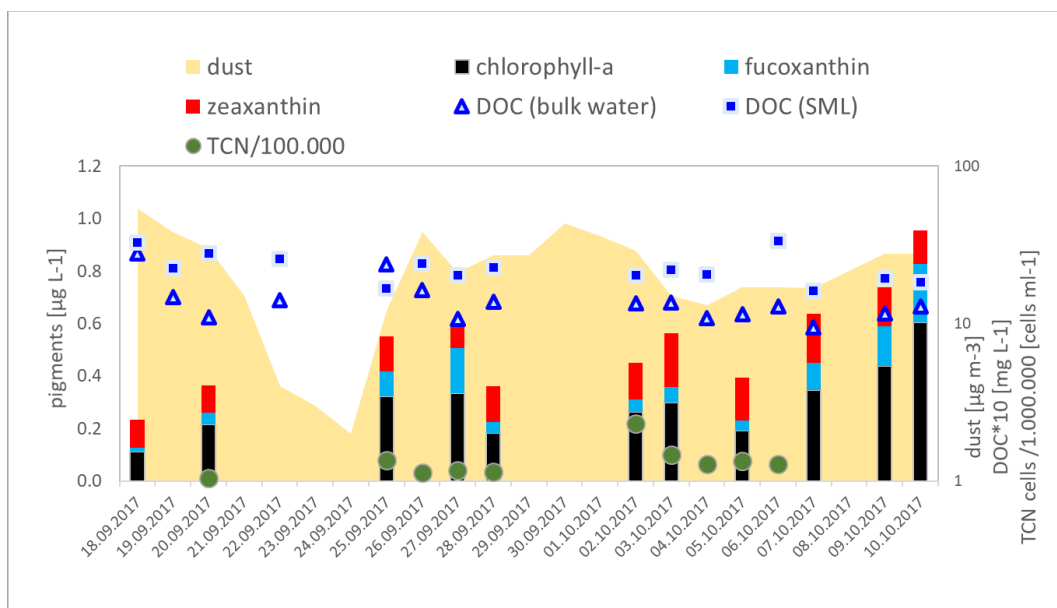


1876  
1877  
1878  
1879  
1880  
1881  
1882  
1883  
1884  
1885  
1886

Figure 12



1887  
1888  
1889  
1890  
1891  
1892  
1893  
1894

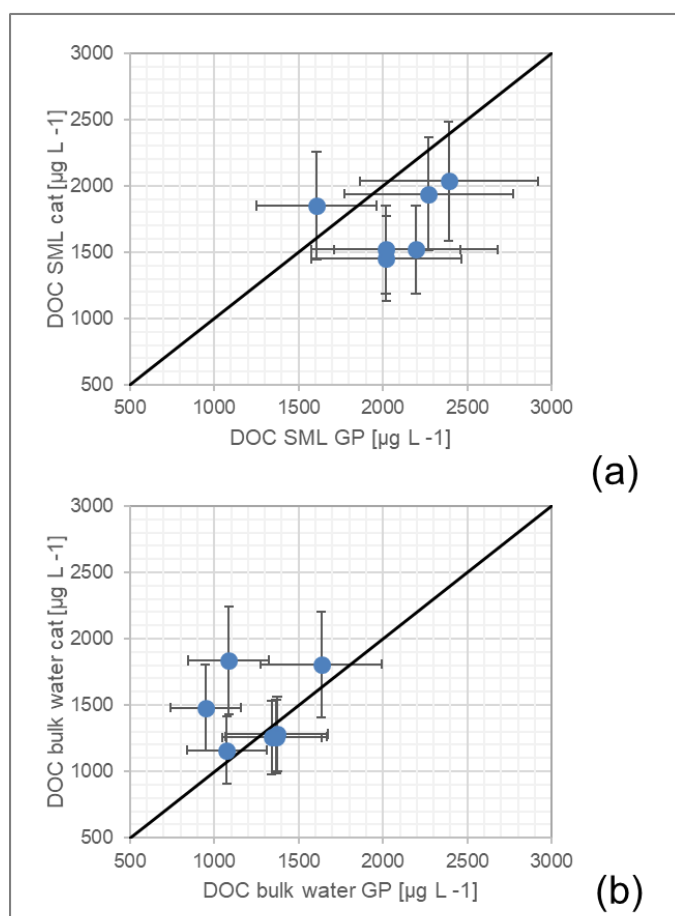


1895  
1896  
1897  
1898  
1899  
1900  
1901  
1902  
1903

Figure 13



1904  
1905  
1906  
1907

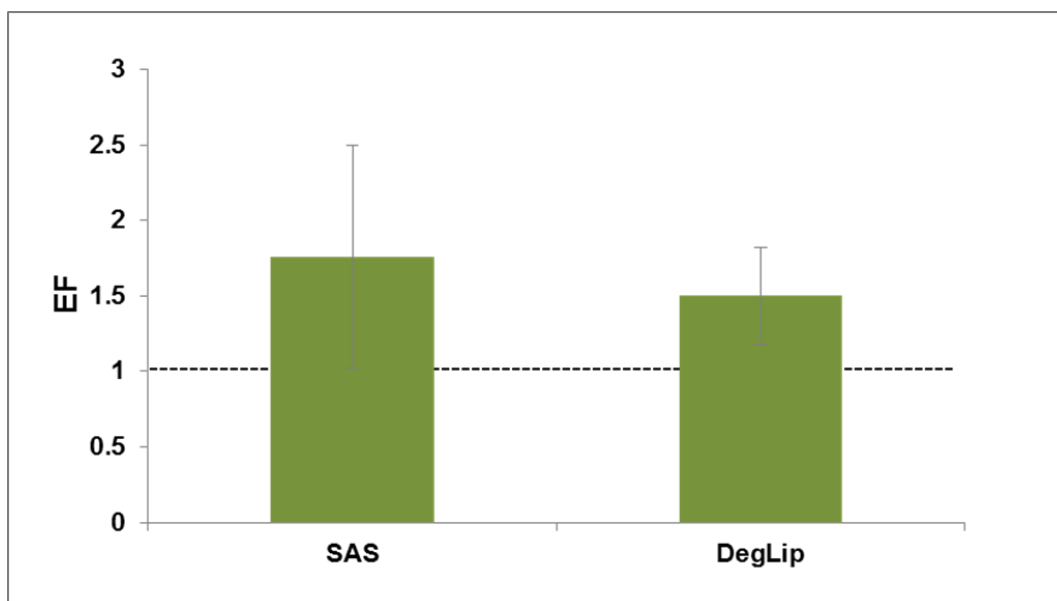


1908  
1909  
1910  
1911  
1912  
1913  
1914

Figure 14



1915  
1916  
1917  
1918  
1919



1920  
1921  
1922  
1923  
1924  
1925  
1926  
1927  
1928  
1929  
1930  
1931

Figure 15



1932

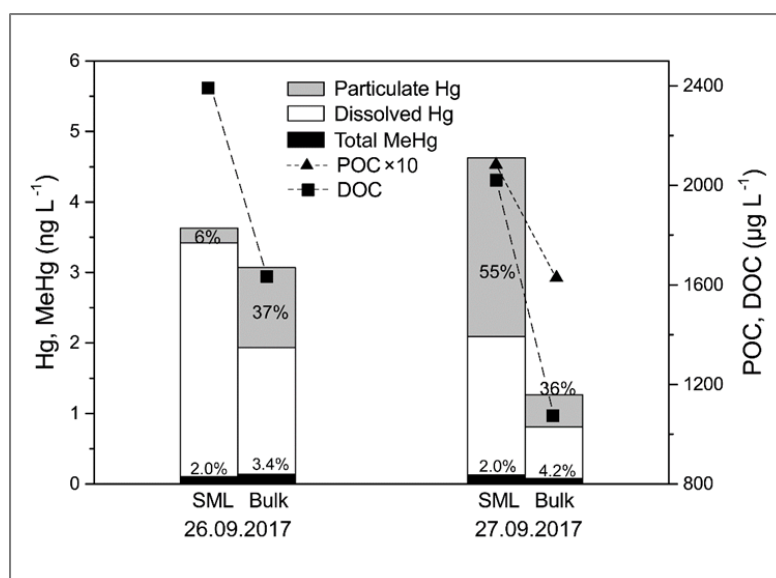
1933

1934

1935

1936

1937



1938

1939

1940

1941

1942

1943

1944

1945

1946

1947

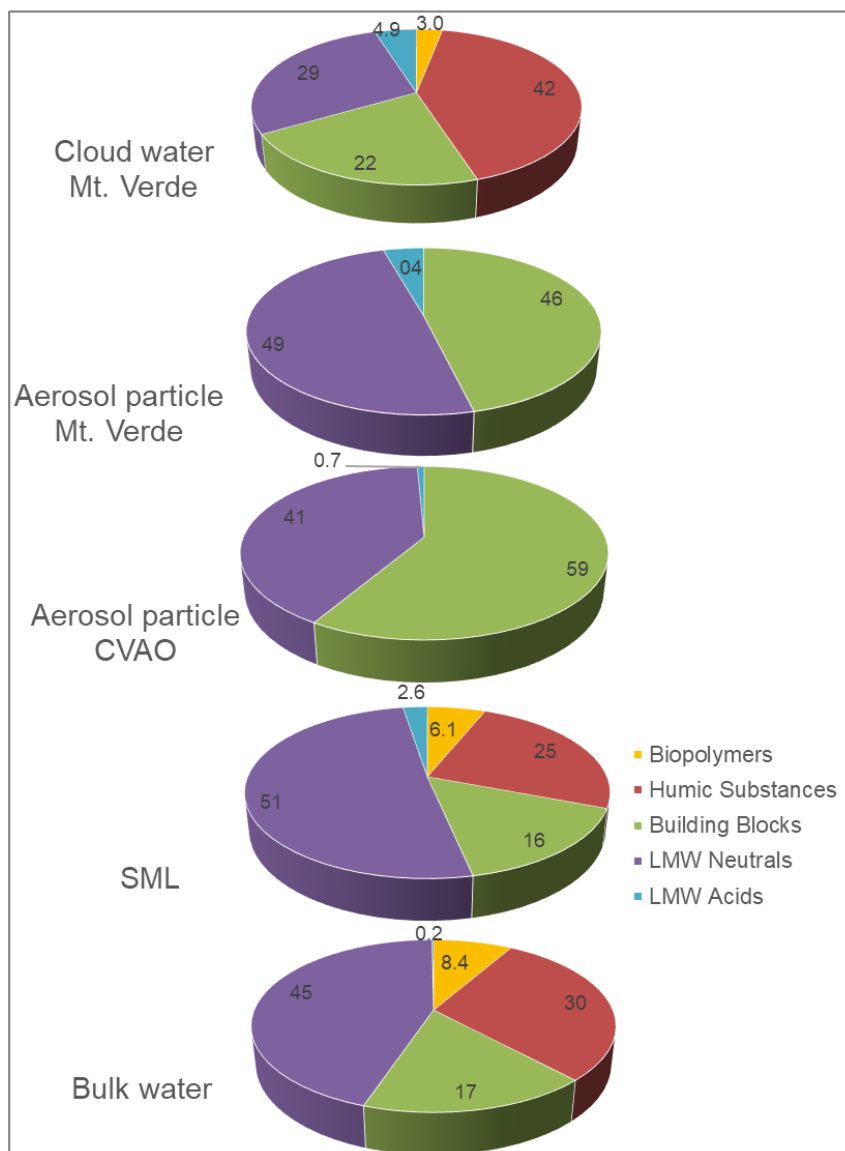
1948

1949

Figure 16



1950



1951

1952

1953

1954

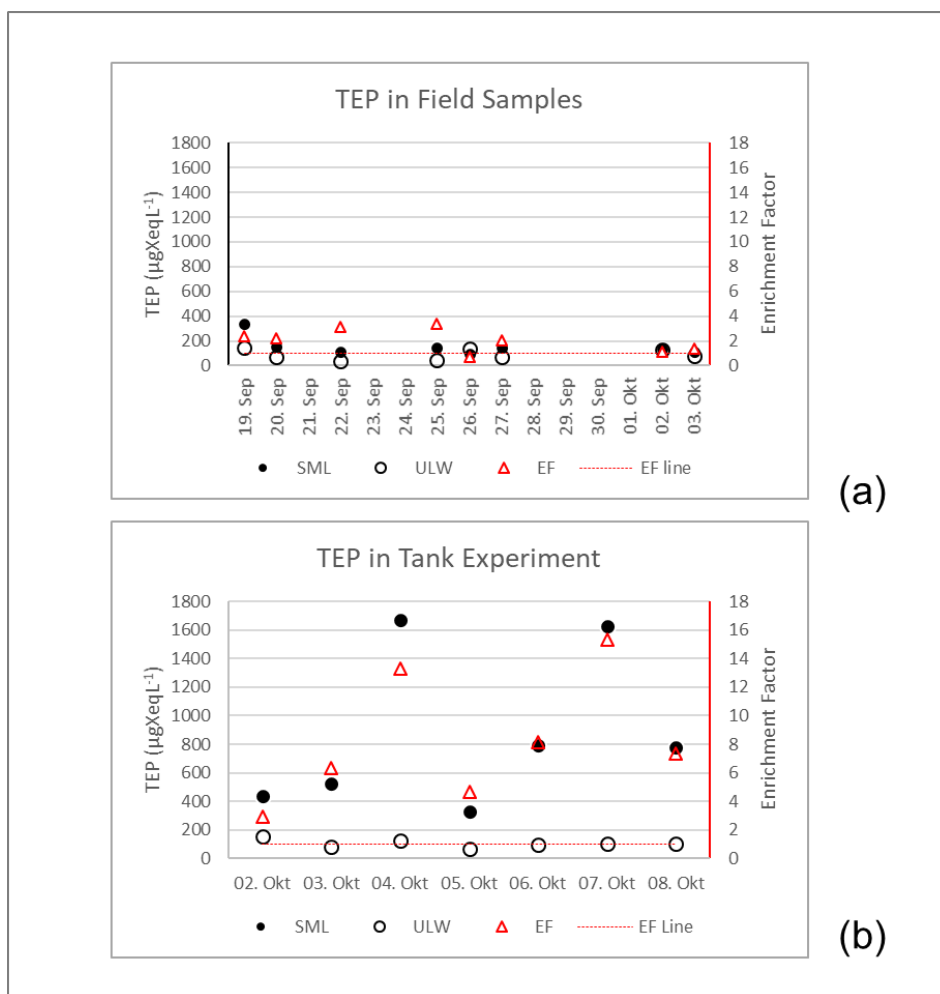
1955

1956

Figure 17



1957



1958

1959

1960

1961

1962

1963

1964

1965

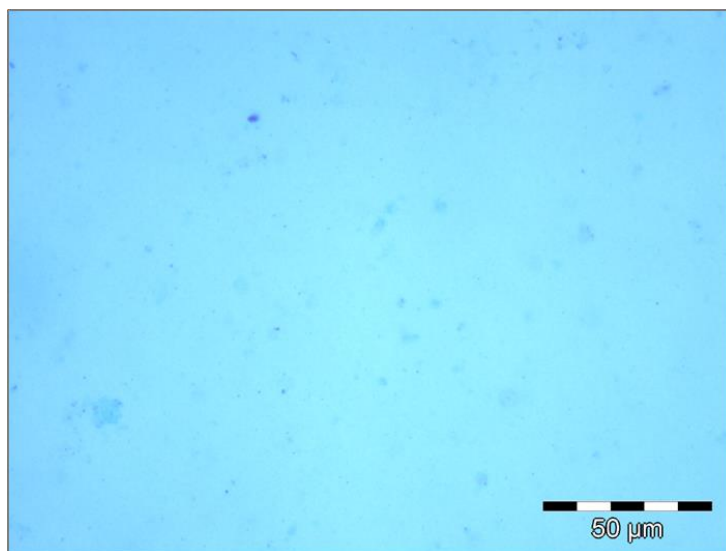
1966

Figure 18



1967

1968



1969

1970

1971

1972

1973

1974

1975

1976

1977

1978

1979

1980

1981

1982

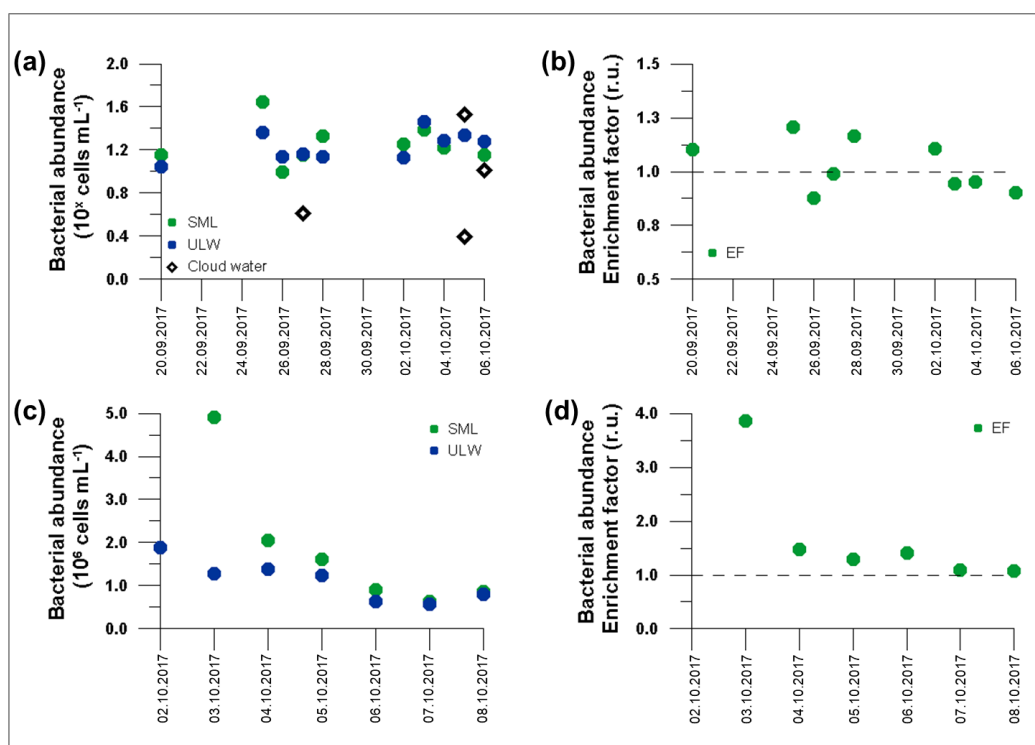
1983

1984

Figure 19



1985  
1986  
1987

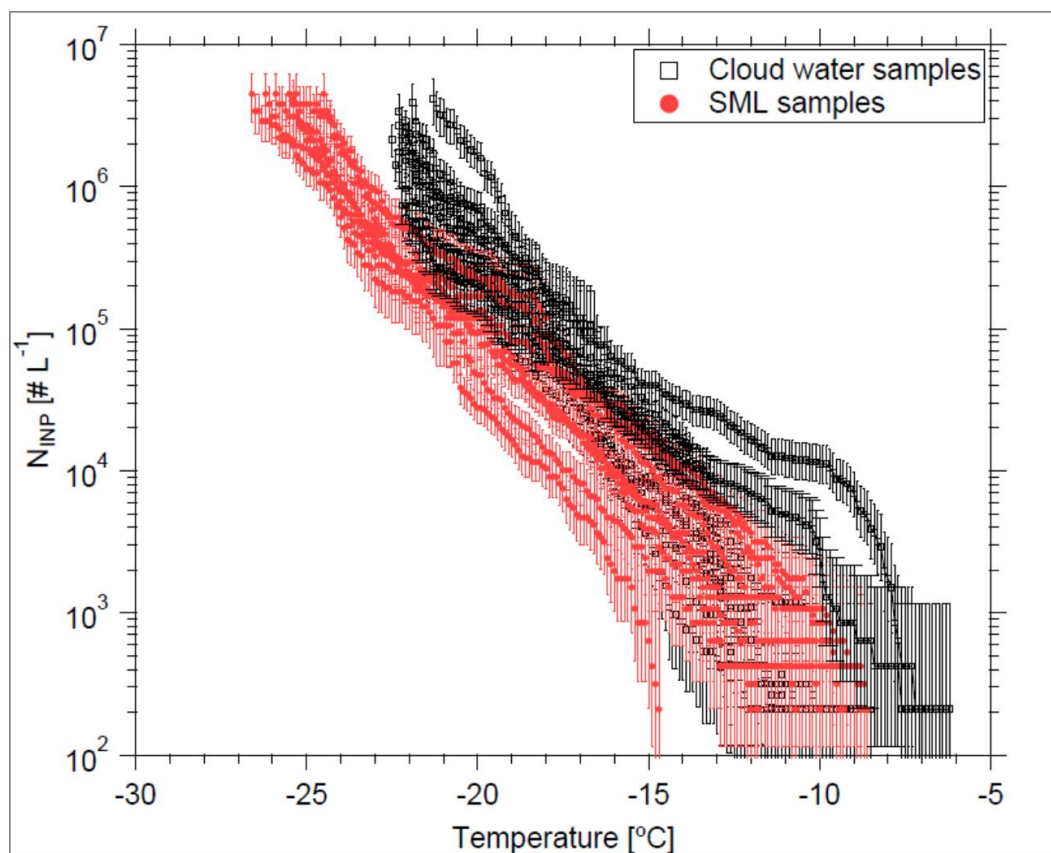


1988  
1989  
1990  
1991  
1992  
1993  
1994  
1995  
1996  
1997  
1998  
1999

Figure 20



2000  
2001  
2002  
2003

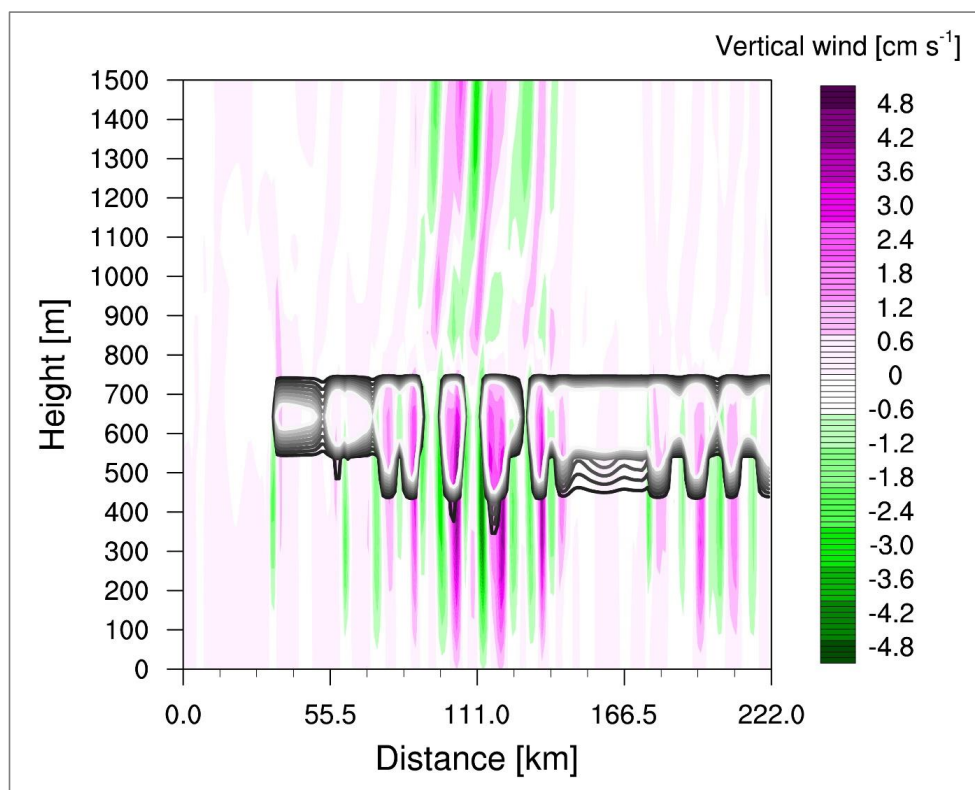


2004  
2005  
2006  
2007  
2008  
2009  
2010  
2011  
2012

Figure 21



2013  
2014  
2015  
2016



2017  
2018  
2019  
2020

Figure 22